

Response to anonymous referee #1

We thank the reviewer for the time spent in reviewing our paper and making very helpful suggestions. We provided a point-by-point response to the reviewer's comments.

1. Anonymous Referee #1

Page 11487, line 12 – What type of events?

Author's response

We are referring here to phenological events such as budburst. We hope that the following changes in the updated manuscript will clarify our statement.

Author's change in manuscript

The following statement on page 11487, line 12 of the discussion paper:

“Some perennial crops like grapevines are already showing a tendency toward earlier events and shortened growth intervals...”

Has been replaced in the updated manuscript with:

“Some perennial crops like grapevines are already showing a tendency toward earlier **budburst** events and shortened growth intervals...”

2. Anonymous Referee #1

Page 11488, line 22 – Do you mean real as opposed from imagined or fictitious?
Please revise.

Author's response

This statement has been clarified in the updated manuscript.

Author's change in manuscript

The following statement on page 11487, line 12 of the discussion paper:

“Notwithstanding some real issues in how best to handle epistemic uncertainties...”

Has been replaced in the updated manuscript with:

“Notwithstanding **important** issues in how best to handle epistemic uncertainties...”

3. Anonymous Referee #1

Page 11493, lines 24–27 – Could these differences be explained by any other phenomena? It might be useful to provide a deeper numerical analysis of this trend. After all, it motivates one half of the analyses presented in the paper.

Author's response

Of course, other phenomena such as transmission losses caused by infiltration through the riverbed (mentioned in the following sentence) may explain the difference between upstream and downstream streamflow. Hence, possible non-linearity in the natural catchment behavior (e.g. surface/groundwater exchanges) may occur between dry and wet periods. Another reason may come from errors in the rating curves of the gauging stations, which can be characterized by non-stationarity in time due to technical changes and/or sensitivity to hydro-climatic variability. These other aspects cannot be easily investigated and this is why the assumption of an increasing impact of irrigation on streamflow was explored through an irrigation model.

However, this is not the only motivation of this paper. Notwithstanding the observed decrease in streamflow, it seems essential to have a more robust model in view of climate and anthropogenic changes in the past and the future. To this end, it is necessary to show that introducing irrigation water-use in the modeling framework improves hydrological simulations without increasing predictive uncertainty. Please see our answer to comment #10 for more details.

4. Anonymous Referee #1

Page 11496, lines 23–24, and Page 11497, lines 15–16 – Some clarification would be welcome: which interval is more consistent with TI model? 1-day or 10-day? also, return flows were supposed to occur within which time step? 1- or 10-day?

Author's response

We thank the reviewer for this comment. Both statements have been clarified in the updated manuscript.

Author's change in manuscript

The following statement on page 11496, lines 23–24 of the discussion paper:

“In this study, all return flows were assumed to come back to the river within each time step.”

Has been replaced in the updated manuscript with:

“In this study, all return flows were assumed to come back to the river within each **10-day** time step.”

The following statement on page 11497, lines 15–16 of the discussion paper:

“This interval was also more consistent with the temperature-index approach used to estimate snowmelt rates.”

Has been replaced in the updated manuscript with:

“This **10-day** interval was also more consistent with the temperature-index approach used to estimate snowmelt rates.”

5. Anonymous Referee #1

Page 11498, lines 8–9 – does this mean that θ_s changes in time?

Author's response

We did not mean to suggest that θ_S changes in time for a given snowpack. Our intention was to mention that θ_S would be expected to be higher in places *where* snowpacks are thick, in comparison to the shallow snowpacks generally found in the dry Andes. We hope that the following changes in the updated manuscript will clarify our statement.

Author's change in manuscript

The following statement on page 11496, lines 23–24 of the discussion paper:

“... θ_S is a parameter quantifying the sensitivity of the snowpack temperature to T_A . A similar representation can be found in other hydrological models, including enhanced versions of SWAT [Fontaine et al., 2002] and SRM [Harshburger et al., 2010]. In general, θ_S is expected to increase with the thickness of the snowpack...”

Has been replaced in the updated manuscript with:

“... θ_S is a parameter quantifying the sensitivity of the snowpack temperature to T_A . As such, θ_S would be expected to be higher in regions characterized by thick snowpacks. A similar representation can be found in other hydrological models, including enhanced versions of SWAT [Fontaine et al., 2002] and SRM [Harshburger et al., 2010].”

6. Anonymous Referee #1

Page 11500, Eq. (10) – Does this mean that the snowpack can either melt or sublimate?

Author's response

Yes, here the snowpack can either melt or sublimate. This modeling choice may seem to oversimplify the physics of snowpacks, yet it was motivated by the absence of true energy balance in the semi-empirical modeling approach used. Moreover, in the dry Andes, the sublimation peak is generally observed before the snowmelt season (e.g. MacDonell et al., 2013). On this point, please see also our modifications to Section 6.

7. Anonymous Referee #1

Page 11510, lines 14–17 – This is a big statement, which merits more discussion. There may be many reasons why this is the case.

Author's response

Agreed. This statement was removed from the updated manuscript.

8. Anonymous Referee #1

Page 11510, lines 24–26 – Not only snow cover duration was underestimated, but also EZ-wide SCA was quite underestimated as well. Given that MODIS has been documented to underestimate fSCA, I wonder if your precip estimates are OK?

Author's response

We agree that uncertainty in precipitation inputs remains large. This point is further discussed in Section 5.3.2. (“Impacts of input data errors”). In mountainous catchments, interpolating precipitation from a sparse station network is always very challenging due to complex

orographic effects, gauge undercatch, sublimation losses and blowing snow transport. Most of the meteorological stations available in the Coquimbo region are located in the river valleys, where precipitation falls mainly as rain, while existing high-elevation stations often do not include appropriately shielded snow sensors.

In this context, the sensitivity of the GR4j model to different ways of interpolating climate forcing in the catchment was investigated in a preliminary paper (Ruelland et al., 2014). Despite the efforts provided to account for orographic effects on precipitation (mean annual precipitation over the study period was assumed to increase by ~ 0.4 m w.e. km^{-1}), numerous precipitation events occurring at high elevations could not be captured by the gauging network ($< 3\,200$ m a.s.l.). As discussed in the paper, precipitation enhancement in the Andes also varies considerably on a year-to-year basis or from one event to another, leading to time-varying errors in the estimation of precipitation inputs when using a constant lapse rate. Overall, this means that precipitation was probably both underestimated and overestimated depending on the event and sub-periods.

9. Anonymous Referee #1

Section 5.1 – This would be more appropriate in the conclusions section (and should be shortened). This may be redundant with what has been said already. I imagine you want to remind the reader what's going on after a rather lengthy methods and results sections, but still...

Author's response

Agreed. This comment was also made by the other referee. We removed Section 5.1 from the updated manuscript and further developed our conclusions (Section 6).

10. Anonymous Referee #1

Section 5.1 – I am a bit puzzled by the reason why should this be a notable result. If flows are not natural, should it be obvious that somehow accounting for water use should improve simulations? Actually, it seems from the results that water use was very stable every year. On the other hand the phenological model is quite complex and requires many (although not all calibrated) parameters. I wonder if you needed all that added complexity to begin with.

Author's response

We thank the referee for this interesting comment. Hydrological processes are often poorly defined at the catchment scale due to the limited number of observations at hand and the integral (low-dimensional) nature of these signals (e.g. streamflow). This makes it relatively easy to over-fit the data by adding new hypotheses to our models, leading to a low degree of *falsifiability* from a Popperian perspective. Therefore the incorporation of new processes into a given model structure should be achieved using as less additional parameters as possible and the same level of mathematical abstraction and process representation as in the original model (as stated in Section 1.4).

In our case, we do agree that the introduction of irrigation water-use in the modeling framework increases the overall number of parameters. However, this increase in model complexity also comes with additional data (observed phenological dates) to reduce the number of degrees of freedom. The referee wonders whether this additional complexity was really necessary in the first place. As a matter of fact, our paper compares three different models of varying complexity. The first one, referred to as Model A, does not incorporate

irrigation water-use (or sublimation losses). It is used as a reference to assess the usefulness of introducing new hypotheses. What we demonstrate is that adding irrigation water-use improves model efficiency and reliability. As such, the increase in complexity appears to be supported by the information content of the available data.

Finally, the referee also mentions the relative stability of irrigation water-use from year to year. However, this stability cannot be taken for granted before running the model. It can only be observed *a posteriori*. Using phenological models also has additional advantages in terms of model robustness under climate- and/or human-induced changes. This is further developed in our response to the next comment.

11. Anonymous Referee #1

Page 11514, lines 1–3 – Please be more specific in terms of why this particular approach is advantageous in this respect. Is this not true of many alternative approaches that simulate natural flows?

Author's response

To our knowledge, most of the other approaches used to ‘naturalize’ influenced streamflow in agricultural catchments do not account for the impacts of climate variability on crop water-use. In practice, the sum of all water access entitlements is often taken as an upper bound for the actual water consumption at the catchment scale and added back to observed streamflow data *before* calibrating a given model (as explained in Section 1.2). In our opinion, these approaches have two main drawbacks. First, they make it difficult to use conceptual hydrological models in climate change impact studies, since changes in temperature patterns are expected to affect both the timing and volume of irrigation water-use. Second, they make it difficult to account for the uncertainty in streamflow predictions attributable to the naturalization process (as briefly explained in Section 1.2).

12. Anonymous Referee #1

Page 11515, lines 3–9 – Is there any way to move beyond the speculative area in this regard? Temperature measurements (although) during spring and summer months exist at high elevation in this region.

Author's response

We do agree that temperature records are now available at high elevations in the Coquimbo region. In the headwaters of the Elqui river catchment, two meteorological stations located above 4000 m a.s.l. have been operated by the CEAZA since 2013–2014. One possibility would be to use these recent observations to calculate a specific lapse rate for each elevation zone used in the model. However, it should be stressed that such temperature data were not available for the 1985–2005 period considered in this paper. Extrapolating recent observations (based on new instruments) to this past period may be a solution, but it may also add further uncertainty to our input data. Therefore we chose to rely on a constant lapse rate as a first approximation.

13. Anonymous Referee #1

Page 11515, line 26 – Are these units correct? I thought that MF multiplied temperature.

Author's response

Agreed. We apologize for this typo which has been corrected in the updated manuscript. The correct unit for melt factors is $\text{mm } ^\circ\text{C}^{-1} \text{ day}^{-1}$.

14. Anonymous Referee #1

Page 11517, line 3 – Please state them here, even if you are discussing them next.

Author's response

Agreed.

Author's change in manuscript

The following statement on page 11517, line 3 of the discussion paper:

“... shedding light on two critical sources of uncertainty.”

Has been replaced in the updated manuscript with:

“... shedding light on two critical sources of uncertainty **related to structural deficiencies and input data errors**.”

15. Anonymous Referee #1

Page 11519, lines 23–24 – I was surprised to not see any first-order water budget estimations that would provide insight into possible input errors. You may consider adding these. Maybe as supplementary material.

Author's response

A first-order water budget was made for this catchment in our previous paper published in HESS (<http://www.hydrol-earth-syst-sci.net/19/2295/2015/hess-19-2295-2015.html>). For brevity's sake we chose not to include it in the current paper.

16. Anonymous Referee #1

Section 6 – The conclusions are somewhat sparse in summarizing the main findings of this work. So much detail is provided in the earlier sections that one would expect to see more defined (if not definitive) conclusions. Most of it is devoted to stating what has been said already about the complexity of the problem at hand, and then it talks about how this study has provided a first step. I would suggest that the authors go back to the introduction-objectives section and relate the conclusions to the objectives stated there. There are two main aspects: incorporating explicitly irrigation demands through a phenological model, and incorporating sublimation into the snow model. The second aspect is not concluded upon, and the first aspect is only glossed over.

Author's response

Agreed. Please see our modifications to the updated manuscript.

17. Anonymous Referee #1

Page 11540, Figure 4 – What is the blue solid line? And the black solid line?

Author's response

Agreed. Regarding the blue solid line, we apologize for this typo which has been corrected in the updated manuscript. The black solid line is also better described in the updated manuscript.

Response to anonymous referee #2

We thank the reviewer for the time spent in reviewing our paper and making very helpful suggestions. We provided a point-by-point response to the reviewer's comments.

1. Anonymous Referee #2

Section 1.2, line 10 – What do you mean by amplified impacts? Larger impacts in relative terms?

Author's response

Yes, that is exactly what we mean. We hope that the following changes in the updated manuscript will clarify our statement.

Author's change in manuscript

The following statement on page 11489, lines 9–10 of the discussion paper:

“During low-flow and drought periods, however, a much greater proportion of natural flow may be abstracted, leading to amplified impacts on the flow regime.”

Has been replaced in the updated manuscript with:

“During low-flow and drought periods, however, a much greater proportion of natural flow may be abstracted, leading to amplified impacts **(in relative terms)** on the flow regime.”

2. Anonymous Referee #2

Section 1.4 – I find it would be useful that the authors more clearly state the scientific question they wish to answer in this article. They could also better explain the complementarity/differences with their other paper recently published in HESS (2015).

Author's response

Agreed. Please see our modifications to Section 1.4 in the updated manuscript.

3. Anonymous Referee #2

Page 11494, line 1 – Are evaporation losses actually significant during routing in the stream channel?

Author's response

Agreed. We did not find any evidence to support this statement. In our opinion, evaporation losses are most likely negligible during streamflow routing. Therefore we removed this point from the updated manuscript.

Author's change in manuscript

The following statement on page 11494, line 1 of the discussion paper:

“Note that transmission losses caused by evaporation and infiltration through the riverbed also reduce streamflow at downstream points, especially during dry periods when the depth of water tables is low.”

Has been replaced in the updated manuscript with:

“Note that transmission losses caused by ~~evaporation and~~ infiltration through the riverbed may also reduce streamflow at downstream points, especially during dry periods when the depth of water tables is low.”

4. Anonymous Referee #2

Page 11494, line 9 – What is “we”? Water equivalent?

Author's response

Yes, “we” is water equivalent in this context. This has been clarified in the updated manuscript.

5. Anonymous Referee #2

Section 3.1 – I wonder whether parts of this section could be put in an appendix. All the details given on the models do not essential to understand the rest of the paper. Though I understand the authors wish to have their model presented in details somewhere, maybe only a summary presenting the general structure of the model and the essential aspects could be left in the main text, and the more detailed description be put in an appendix or supplementary material.

Author's response

We thank the reviewer for this important suggestion. Please see our modifications in the updated manuscript.

6. Anonymous Referee #2

Page 11500, Eq. 12 – Should PEGR4J be the maximum of this quantity and zero?

Author's response

Agreed. Eq. (12) was clarified in the updated manuscript, taking zero as a lower bound.

7. Anonymous Referee #2

Page 11507, line 11-13 – These aspects may not be meaningful for readers not familiar with DREAM.

Author's response

Agreed. These details have been removed from the updated manuscript to make the reading easier for all readers.

8. Anonymous Referee #2

Page 11510, line 18-29 – Not sure this part is very useful.

Author's response

We think this part is useful for at least two reasons. First, it shows that the Snow Accumulation and Ablation (SAA) model did not accumulate snow from one year to another, which is consistent with MODIS-based inter-annual pattern of snow cover in the catchment. Second, it shows that the model generally failed to accurately reproduce the observed variations in snow cover areas in the upper zones, which questions precipitation estimates in the catchment, as underlined by the other referee.

As discussed in Section 5.3.2 (“Impacts of input data errors”), interpolating precipitation from a sparse station network is always very challenging due to complex orographic effects, gauge undercatch, sublimation losses and blowing snow transport. Most of the meteorological stations available in the Coquimbo region are located in the river valleys, where precipitation falls mainly as rain, while existing high-elevation stations often do not include appropriately shielded snow sensors. Despite the efforts provided to account for orographic effects on precipitation, numerous precipitation events occurring at high elevations cannot be captured by the gauging network used to interpolate precipitation. Moreover, as discussed in the paper, precipitation enhancement in the Andes vary considerably on a year-to-year basis or from one event to another, leading to time-varying errors in the estimation of precipitation inputs when using a constant lapse rate. This means that precipitation was probably both underestimated and overestimated depending on the event and sub-periods.

9. Anonymous Referee #2

Page 11511, lines 22-25 – I did not fully understand the link between the model parameters and the use of irrigation data.

Author's response

Agreed. We hope that the following changes in the updated manuscript will clarify our statement.

Author's change in manuscript

The following statement on page 11511, lines 22–25 of the discussion paper:

“Likewise, additional checks performed with Models B and C showed that the strong correlation between X2 and X3 observed for Model C was mainly due to the incorporation of irrigation water-use in the modeling framework.”

Has been replaced in the updated manuscript with:

“Likewise, additional checks performed with Models B and C showed that the incorporation of irrigation water-use in Model C led to a strong correlation between X2 and X3, which questions the internal consistency of the Runoff production and routing module when increasing the model complexity.”

10. Anonymous Referee #2

Section 5.1 – I find this sub-section would better fit in the concluding section.

Author’s response

Agreed. This comment was also made by the other anonymous referee. Part of this sub-section was moved to Section 6 (“Conclusion and prospects”), and part of it was removed from the updated manuscript. Please see our modifications in the updated manuscript.

11. Anonymous Referee #2

Page 11514, line 16 – Formulation not fully clear. May be rephrased.

Author’s response

Agreed. We hope that the following changes in the updated manuscript will clarify our statement.

Author’s change in manuscript

The following statement on page 11514, line 16 of the discussion paper:

“This runs counterintuitive to the idea that shallow snow packs such as those observed in the region should have a low thermal inertia.”

Has been replaced in the updated manuscript with:

“This finding seems a contradiction of the idea that shallow snow packs such as those observed in the region should have a low thermal inertia.”

12. Anonymous Referee #2

Section 5.3.1 – I found this discussion not very convincing. It remains quite general and discusses hypotheses that cannot be checked here. Therefore it is not conclusive. The section may be shortened or removed.

Author’s response

While we fully agree that such hypotheses cannot be checked here, they should not be considered as conclusive statements. Our intention here is mainly to discuss the structural adequacy of our models for the representation of semi-arid, Andean catchments. We

understand that the version reviewed by the referee may seem too conclusive, and therefore we provided several modifications in the updated manuscript to qualify our statements and better emphasize the hypothetical nature of this discussion. The Section (now 5.2.1) was also significantly shortened.

13. Anonymous Referee #2

References – The authors could cite their recent paper published in PIAHS (<http://www.proc-iahs.net/371/203/2015/piahs-371-203-2015.html>) and explain the complementarity of this new paper compared to that already published paper on the same topic.

Author's response

Agreed. Please see our modifications to Section 1.4 in the updated manuscript.

14. Anonymous Referee #2

Table 1 – In the caption, it should be “third” and “fourth” instead of “second” and “third” respectively. The heading of the third column may be “Meaning”.

Author's response

Agreed. We apologize for this typo which has been corrected in the updated manuscript. Also, the term “signification” has been replaced with the term “meaning”.

15. Anonymous Referee #2

Table 2 – Please indicate the units of RMSE (days), NSE (-) and Bias (days).

Author's response

Agreed. Please see our modifications in the updated manuscript.

16. Anonymous Referee #2

Table 3 – Please indicate the units of parameters.

Author's response

Agreed. Please see our modifications in the updated manuscript.

17. Anonymous Referee #2

Table 4 – Indicate units of criteria.

Author's response

Agreed. Please see our modifications in the updated manuscript.

18. Anonymous Referee #2

Figure 2 – When printed black and white, the green and blue boxes appear the same. Maybe find another way to differentiate more clearly the hydrological and irrigation modules on the figure.

Author's response

Agreed. Colors of the different boxes have been modified so as to be clearly differentiable when printed in grey levels.

19. Anonymous Referee #2

Figures 6 and 12 – Maybe use more different line types (e.g. dashed line) so that the graphs can be more easily understood when printed black and white.

Author's response

Agreed. Please see our modifications in the updated manuscript.

20. Anonymous Referee #2

Figure 11 – Top right graph: I did not understand what is meant by “water level variations (%)”.

Author's response

This point was clarified in the updated manuscript. The level of water in each model store is expressed as a percentage of the maximum storage capacity (given by parameters $X1$ and $X3$).

21. Anonymous Referee #2

Figure 12 – In the blue series, there are some suspect data, typically a sudden drop in the year 1988 or almost constant values over 1998-2000. How can this be interpreted?

Author's response

Such data are difficult to interpret because the actual water withdrawals in the catchment remain unknown. The net surface-water withdrawals (SWW) used here are derived from a ‘water rights’ database provided by the local stakeholders for the 1985–2005 period. It is worth noting, however, that SWW data reflect more a level of water availability in the catchment than the actual water consumption in the vineyards. These data may also indicate sudden changes in the management of water resources at the whole catchment scale (i.e. for the Elqui River catchment) which do not necessarily affect irrigation requirements at the local scale. In particular, the constant values observed over 1998–2000 may reflect the stability of water availability following the El Niño event of 1997–1998. The sudden drop in 1988 is most likely an error (this point was not removed because we are not sure about it and because these data are used only for comparison). Please see our modifications in the updated manuscript.

1 Reliability of lumped hydrological modeling in a semi-arid 2 mountainous catchment facing water-use changes

3
4 P. HUBLART^{1,7}, D. RUELLAND², I. GARCÍA DE CORTÁZAR-ATAURI³, S.
5 GASCOIN⁴, S. LHERMITTE⁵ and A. IBACACHE⁶

6 [1] {UM2, UMR HydroSciences Montpellier, Montpellier, France}

7 [2] {CNRS, UMR HydroSciences Montpellier, Montpellier, France}

8 [3] {INRA, US 1116 AGROCLIM, Avignon, France}

9 [4] {CNRS, CESBIO, UMR 5126, Toulouse, France}

10 [5] {KU LEUVEN, Division of Geography, Leuven, Belgium}

11 [6] {INIA, Colina San Joaquín s/n, La Serena, Chile}

12 [7] {CEAZA, Raúl Bitrán s/n, La Serena, Chile}

13 Correspondence to: P. Hublart (p.hublart@gmail.com)

14 15 16 **Abstract**

17
18 This paper explores the reliability of a hydrological modeling framework in a mesoscale
19 (1515 km²) catchment of the dry Andes (30°S) where irrigation water-use and snow
20 sublimation represent a significant part of the annual water balance. To this end, a 20-year
21 simulation period encompassing a wide range of climate and water-use conditions was
22 selected to evaluate three types of integrated Models referred to as A, B and C. These Models
23 share the same runoff generation and routing module but differ in their approach to snowmelt
24 modeling and irrigation water-use. Model A relies on a simple degree-day approach to
25 estimate snowmelt rates and assumes that irrigation impacts can be neglected at the catchment
26 scale. Model B ignores irrigation impacts just as Model A but uses an enhanced degree-day
27 approach to account for the effects of net radiation and sublimation on melt rates. Model C
28 relies on the same snowmelt routine as Model B but incorporates irrigation impacts on natural
29 streamflow using a conceptual irrigation module. Overall, the reliability of probabilistic
30 streamflow predictions was greatly improved with Model C, resulting in narrow uncertainty
31 bands and reduced structural errors, notably during dry years. This model-based analysis also

32 stressed the importance of considering sublimation in empirical snowmelt models used in the
33 subtropics, and provided evidence that water abstractions from the unregulated river is
34 impacting on the hydrological response of the system. This work also highlighted areas
35 requiring additional research, including the need for a better conceptualization of runoff
36 generation processes in the dry Andes.

37

38

39 **1. Introduction**

40

41 Mountains act as natural water towers in many semi-arid regions. Glaciers and seasonal
42 snowpack in the uplands serve as reservoirs, accumulating water during the winter and
43 sustaining streams and aquifers during the spring and summer. This reduces streamflow
44 variability in the lowlands and provides local communities with the opportunity to develop
45 agricultural systems based on regular water supplies. Irrigation often represents a large part of
46 crop water-use in these areas due to the dry conditions that prevail during the growing season
47 [Siebert and Döll, 2010].

48 This makes such systems highly vulnerable to projected changes in climate conditions, for
49 at least two reasons. First, warmer temperatures will reduce the fraction of precipitation
50 falling as snow and tend to accelerate snowmelt, leading to earlier and reduced spring peak
51 flows and increased winter flows [Adam et al., 2009; Sproles et al., 2013]. Reduced summer
52 and fall flows could in turn significantly impact water availability for irrigation purposes.
53 Second, higher temperatures in the valleys will affect the timing of phenological events
54 [Cleland et al., 2007], which drive the seasonal pattern of crop water needs. Some perennial
55 | crops like grapevines are already showing a tendency toward earlier [budburst](#) events and
56 shortened growth intervals in many regions of the world [Jones et al., 2005; Duchêne et al.,
57 2010a]. Vineyards located in semi-arid mountainous areas are particularly exposed, owing to
58 high diurnal temperature variations and overall sub-optimal growing temperatures [Caffarra
59 and Eccel, 2011]. It has also been noted that elevated temperatures may adversely affect the
60 ability to meet chilling requirements during the crop dormancy [Webb et al., 2007].

61 Thus, the future of agricultural systems in snow-dominated, semi-arid catchments relies on
62 our ability to anticipate the complex relationships between climate conditions, snowmelt
63 timing, water availability and crop water-use.

64

1.1. Advantages and limitations of current conceptual precipitation-runoff models

To understand and forecast the response of hydrological systems, hydrologists often rely on numerical catchment models known as ‘conceptual precipitation-runoff models’. Precipitation inputs are processed into runoff through a number of inter-connected water stores representing different aspects of the system's behavior (e.g. slow vs. fast responses, surface-water vs. groundwater compartments). In general, relatively simple structures are used, in which typically less than 10 parameters require calibration against physically observable responses (e.g. streamflow data) [Wagner et al., 2001]. Such models also have low data and computer requirements, making them especially attractive in data-scarce areas such as remote mountainous catchments. As a result, they are being increasingly used to evaluate the potential impacts of land-use and/or climate changes on the capacity to meet agricultural water demands [e.g. Merritt et al., 2004; Collet et al., 2015; Fabre et al., 2015a].

The conclusions drawn from these models, however, are naturally bounded by a range of uncertainty arising from multiple sources of error and approximations. This includes the impacts of input data errors, numerical approximations, structural inadequacies and model non-uniqueness. Parameter instability under changing climate and/or anthropogenic conditions represents an additional source of uncertainty that may be difficult to distinguish from parameter equifinality in the absence of uncertainty analysis [Seibert and McDonnell, 2010; Brigode et al., 2013]. Such limitations remain largely overlooked in many impact studies. Instead, it is often assumed that the uncertainty associated with climate and/or water-use scenarios greatly outweighs that arising from the modeling process itself. From a water management perspective, however, the added value of precipitation-runoff models lies not simply in their ability to provide accurate streamflow predictions but also in the systematic examination of the uncertainty surrounding these predictions and the ultimate decision being addressed [Ajami et al., 2008].

One of the most effective means of providing such information is through the use of Bayesian inference methods. Notwithstanding ~~some~~ real important issues in how best to handle epistemic uncertainties, and whether probability theory is the right tool to use [Beven et al., 2011; Montanari, 2011], formal Bayesian approaches offer the opportunity to test the reliability of model predictions through a series of posterior diagnostics. This, in turn, provides a meaningful way to discuss the relative merits of competing model structures or different versions of the same model. Very often, structural inadequacies can be partially

99 alleviated by comparing alternative representations of the processes at work. This paper
100 addresses two specific issues pertaining to the use of conceptual models in semi-arid
101 catchments where the effects of irrigation water-use and snow sublimation cannot be
102 dismissed *a priori*.

103

104 **1.2. Potential impacts of water abstraction and irrigation water-use**

105

106 The first issue deals with water abstraction for irrigation, which has many potential impacts
107 on hydrological processes, including changes in groundwater recharge [Scanlon et al., 2006]
108 and low-flow characteristics [Yang et al., 2010]. In arid and semi-arid catchments, these
109 impacts may be hard to quantify because a high degree of temporal and spatial variability in
110 climate conditions often mask anthropogenic trends [Kim et al., 2007]. During low-flow and
111 drought periods, however, a much greater proportion of natural flow may be abstracted,
112 leading to amplified impacts (in relative terms) on the flow regime. The poor performance of
113 most conceptual models during these critical periods is a well-recognized issue in the
114 hydrological research community and many studies have formulated different approaches
115 towards improving low-flow simulations [e.g. Smith et al., 2010; Staudinger et al., 2011;
116 Pushpalatha et al., 2011]. Yet, most of these studies have been concerned mainly with
117 undisturbed river systems. The impacts of river damming and regulation have also been
118 studied extensively, but there is a surprising dearth of work regarding the effects of water
119 abstraction from unregulated streams.

120 A common approach to remove such effects in model building and evaluation is to rely on
121 ‘naturalized’ streamflow data [e.g. Ashagrie et al., 2006]. This requires detailed information
122 on surface or ground water withdrawals and irrigation water-use, which is rarely available. In
123 practice, the sum of all water access entitlements is often taken as an upper bound for the
124 actual water consumption at the catchment scale, and added back to observed streamflow data
125 before calibrating a given model. Yet, farmers may not withdraw their full entitlement all year
126 long and a significant part of water withdrawals actually return to the river system within a
127 few days or weeks due to conveyance and field losses. In theory, ignoring these return flows
128 would lead to overestimating natural streamflow. But in reality, it can be very difficult to
129 disentangle the relative influence of epistemic errors in streamflow estimates (rating curve
130 errors, unknown return flows) and input data (precipitation, temperature, potential
131 evapotranspiration). Therefore, for a proper assessment of model reliability, streamflow
132 naturalization should be considered an integral part of the modeling process and explicitly

133 recognized as an additional source of imprecision in streamflow predictions [Hughes and
134 Mantel, 2010; Hublart et al., 2015a].

135

136 **1.3. Potential impacts of sublimation losses**

137

138 The second issue addressed by this paper concerns the means by which snowmelt inputs are
139 obtained in snow-dominated, semi-arid catchments. Many studies rely on empirical degree-
140 day approaches, in which air temperature is taken as a reasonable proxy for the energy
141 available for melt [Ohmura, 2001]. Melt rates are assumed to be linearly related to air
142 temperature by a constant of proportionality known as the ‘melt factor’, which can vary on a
143 seasonal basis [Hock, 2003]. Enhanced degree-day methods are sometimes implemented to
144 include the effects of additional variables such as solar radiation or wind speed. However, by
145 focusing exclusively on melt rates, such approaches can prove highly misleading where
146 sublimation losses represent a large part of ablation rates. This is generally the case in semi-
147 arid areas located around 30°S and 30°N.

148 Sublimation rates in the subtropics are expected to be high as a result of very low relative
149 humidity and intense solar radiation during most of the year. In the dry Andes, for instance,
150 Gascoin et al. [2013] found that sublimation losses represented more than 70% of the total
151 ablation simulated by a physically-based model in the instrumented site of Pascua-Lama
152 (1043 km², 2600–5630 m a.s.l.). Similar results were also obtained by experimental studies
153 conducted on small glaciers of the same region [MacDonell et al., 2013]. In the Northern
154 Hemisphere, Schulz and de Jong [2004] attributed up to 44% of annual snow ablation to
155 sublimation in a 140 km² catchment of the High Atlas range (2000–4000 m a.s.l.). It is
156 becoming increasingly recognized that failure to account for sublimation losses in commonly-
157 used temperature-index methods can impair model performance, distort parameter
158 identification and question the reliability of snowmelt estimates under higher temperatures
159 [e.g. Boudhar et al., 2009; Ayala et al., 2015].

160

161 **1.4. Objectives**

162

163 Ideally, the incorporation of new processes into a given model structure should be achieved
164 using the same level of mathematical abstraction and process representation as in the original
165 model. Blöschl and Montanari [2010] insisted that “a better understanding of the hydrological
166 processes should not necessarily translate into more complex models used in impact studies”.

167 Indeed, maintaining low-dimensional, holistic modeling approaches is essential to constrain
168 parameter uncertainty and help the modelers focus on understanding the main drivers of
169 hydrological change.

170 This paper investigates one possible way of integrating the effects of irrigation water-use
171 and snow sublimation into a parsimonious, catchment-scale modeling framework. ~~These Such~~
172 processes are typically not accounted for in currently available precipitation-runoff models.
173 Particular attention is paid to the representation of changes in irrigated areas and crop
174 varieties over time. The method is tested in a snowmelt-fed catchment of the Coquimbo
175 region ~~(Chile), in Chile,~~ which is currently facing one of the worst droughts in its recorded
176 ~~history [Salinas et al., 2015]. This semi-arid region is currently facing one of the worst~~
177 ~~droughts in its recorded history, causing a significant decrease in water availability for~~
178 ~~agriculture [Salinas et al., 2015]. In the same catchment, Hublart et al. (2015a) attempted to~~
179 ~~reduce structural uncertainty in a non-probabilistic way by comparing 72 alternative models~~
180 ~~derived from the same modular framework. However, the potential effects of irrigation and~~
181 ~~sublimation were not included in this multiple-hypothesis framework, thereby limiting its~~
182 ~~ability to cope with climate and anthropogenic changes. Hublart et al. (2015b) provided a first~~
183 ~~attempt to incorporate these two processes in a precipitation-runoff model, but several~~
184 ~~important aspects, such as the quantification of model uncertainty and the quality of snowmelt~~
185 ~~simulations, remained outside the scope of their study. Compared to this previous paper, the~~
186 ~~present study makes use of (1) extended calibration and validation periods to encompass a~~
187 ~~wider range of climate and water-use conditions, (2) formal Bayesian theory to quantify~~
188 ~~predictive uncertainty in a probabilistic way, and (3) remotely-sensed snow-cover data to~~
189 ~~evaluate the internal consistency of the snow module.~~

190

191

192 **2. Study area and data**

193

194 **2.1. General setting**

195

196 **2.1.1. Physical landscape**

197

198 The Claro River catchment is a semi-arid, mountainous catchment located in North-Central
199 Chile (30°S). It drains an area of about 1 515 km² characterized by a series of granitic
200 mountain blocks interspersed with steep-sided valleys. Elevations range from 820 m a.s.l. at

201 the catchment outlet in Rivadavia to approximately 5500 m a.s.l. near the border with
202 Argentina (Fig. 1a). Above 3000 m a.s.l., repeated glaciations and the continuous action of
203 frost and thaw throughout the year have caused an intense shattering of the exposed rocks,
204 leaving a landscape of bare rock and screes almost devoid of soil. The valley-fill material
205 consists of mostly unconsolidated glaciofluvial and alluvial sediments mantled by generally
206 thin soils (< 1 m) of sandy to sandy-loam texture. Natural vegetation outside the valleys is
207 extremely sparse and composed mainly of subshrubs (e.g. *Adesmia echinus*) and cushion
208 plants (e.g. *Laretia acaulis*) with very low transpiration rates [Squeo et al., 1993; Kalthoff et
209 al., 2006]. In the lower part of the catchment, vineyards and orchards cover most of the valley
210 floors and lower hill slopes, where they benefit from a unique combination of clear skies, high
211 diurnal temperature variations and overall dry conditions during the growing season. The
212 Claro River originates from a number of small, snowmelt-fed tributaries flowing either
213 permanently or seasonally in the mountains.

214

215 **2.1.2. Climate**

216

217 Most of the annual precipitation falls as snow during typically 2 or 3 winter storms [Favier et
218 al., 2009], when the South Pacific High reaches its northernmost position (June–August).
219 Mean annual precipitation ranges from approximately 100 mm at the catchment outlet
220 (Rivadavia) to 670 mm in the High Cordillera [Bourgin et al., 2012]. The annual snow cover
221 duration estimated from MODIS snow-covered area (SCA) data (see Sect. 2.2.) ranges from
222 less than 20–40 days at low elevations (< 2000 m a.s.l.) to about 160–180 days at high
223 elevations (> 4000 m a.s.l.), where sublimation is expected to be the dominant cause of
224 ablation [Gascoin et al., 2013; MacDonell et al., 2013]. In the dry Andes, net shortwave
225 radiation represents the dominant source of energy available for melt and sublimation
226 [Pelliciotti et al., 2008].

227 At the inter-annual timescale, the El Niño Southern Oscillation (ENSO) represents the
228 largest source of climate variability [Montecinos and Aceituno, 2003]. Anomalously wet (dry)
229 years in the region are generally associated with warm (cold) El Niño (La Niña) episodes and
230 a simultaneous weakening (strengthening) of the South Pacific High. It is worth noting,
231 however, that some very wet years in the catchment can also coincide with neutral to weak La
232 Niña conditions, as in 2000–2001, while several years of below-normal precipitation may not
233 exhibit clear La Niña characteristics [Verbist et al., 2010]. These anomalies may be due to
234 other modes of climate variability affecting the Pacific basin on longer timescales. The

235 Interdecadal Pacific Oscillation (IPO), in particular, has been shown to modulate ENSO's
236 influence according to cycles of 15 to 30 years [Schulz et al., 2011]. Figure 1c shows a
237 sustained decrease in mean annual streamflow since the mid-1990s, which could be associated
238 with a shift in the IPO phase around 1998.

239

240 **2.1.3. Agricultural activity**

241

242 Grape growing is by far the main agricultural activity in the catchment. All grapes are grown
243 to be exported as early-season table grapes or processed into a brandy-like national drink
244 known as *pisco*. Reliable water supplies are critical to satisfy crop water needs in the summer,
245 since precipitation events occur mostly at high elevations or outside the growing season.
246 Irrigation water is diverted at multiple locations along the river's course and conveyed to the
247 fields through a complex network of open, mostly unlined canals. The amount of water
248 diverted from the river depends on both historical water rights and current water availability.
249 Table varieties are mostly drip-irrigated while pisco varieties remain largely furrow-irrigated.

250 Irrigated areas in the Claro River catchment have increased by about 200% between 1985
251 and 2005 (Fig. 1b). This expansion has been limited by both water and agricultural land
252 availability, and irrigated areas currently represent less than 5% of the total catchment area. A
253 rough estimate of the effects of increased irrigated areas on mean annual streamflow can be
254 obtained by looking at the difference in discharge measured at Rivadavia (downstream from
255 cultivated areas) and that measured at Cochiguaz and Alcohuz (upstream from cultivated
256 areas) (Fig. 1c). Note that transmission losses caused by ~~evaporation and~~ infiltration through
257 the riverbed may also reduce streamflow at downstream points, especially during dry periods
258 when the depth of water tables is low.

259

260 **2.2. Materials**

261

262 **2.2.1. Hydro-climate data**

263

264 Precipitation and temperature data were interpolated from respectively 12 and 8 stations to a 5
265 × 5 km grid using an inverse distance squared weighting [Ruelland et al., 2014]. Orographic
266 effects on precipitation were considered using the approach described in Valéry et al. [2010a]
267 with a correction factor of $6.5 \cdot 10^{-4} \text{ m}^{-1}$ (determined by sensitivity analysis), resulting in a
268 gradient of around 0.4 m water equivalent per km w.e. km⁻¹. For temperature, a constant lapse

269 rate of $-6.0^{\circ}\text{C km}^{-1}$ was estimated from the observed data. Daily streamflow data were
270 extracted from the Chilean *Dirección General de Aguas*' database.

271 In addition, remotely-sensed data from the MODerate resolution Imaging
272 Spectroradiometer (MODIS) sensor were introduced to estimate the seasonal patterns of
273 fractional snow-covered areas (F_{SCA}) over a 12 year period (2000–2011). Daily snow cover
274 products retrieved from NASA's Terra (MOD10A1) and Aqua (MYD10A1) satellites were
275 combined into a single, composite 500 m resolution product to reduce the effect of swath gaps
276 and cloud obscuration. The remaining data voids due to cloud cover or missing data were
277 subsequently filled using a linear temporal interpolation method, where a pixel was classified
278 as snow/land depending on the closest previous/next observation of snow/land.

279

280 **2.2.2. Agricultural data**

281

282 Two different grapevine varieties were selected to represent phenological patterns in the
283 valleys, namely: Flame Seedless (for table grapes) and Moscatel Rosada (for pisco grapes).
284 Phenological observations for these two varieties were carried out over a 10-year period
285 (2003–2012) at the *Instituto de Investigaciones Agropecuarias* (INIA), located a few
286 kilometers downstream from the catchment outlet. Grapevines were trained using an overhead
287 trellis system and fully irrigated during the whole growing season. The experiment kept track
288 of three major events: budburst (BB), full bloom (FB) and the beginning of harvest (HV).
289 Budburst was defined as the moment when the first leaf tips become visible and full bloom as
290 the moment when 80% of the flower caps are off. The beginning of harvest depends on the
291 intended use of the grapes. Table varieties require lower sugar contents ($\sim 16^{\circ}$ Brix) than
292 those dedicated to the production of pisco (22° Brix), which are generally harvested a few
293 months later [Ibacache, 2008].

294 A database of water access entitlements was used to estimate the total volume of water
295 licensed for abstraction in the catchment. This included a time series of monthly restrictions to
296 these entitlements issued by the *Dirección General de Aguas* during prolonged dry periods.

297

298

299 **3. Methods**

300

301 **3.1. Modeling framework**

302

303 In this paper we developed and compared three different models. These differed in their
304 approach to snowmelt and irrigation modeling. The first one, referred to as ‘Model A’, used a
305 simple degree-day approach to estimate snowmelt rates while neglecting the effects of
306 irrigation water-use (IWU) at the catchment scale. The second one, referred to as ‘Model B’,
307 ignored IWU effects just as Model A but relied on an enhanced degree-day approach to
308 account for the effects of net radiation and sublimation on melt rates. The third one, referred
309 to as ‘Model C’, used the same snowmelt routine as Model B and incorporated IWU effects
310 on natural streamflow using a conceptual irrigation module.

311 Figure 2 shows a block diagram of this modeling framework. The blue blocks refer to the
312 hydrological part of the framework shared by the three Models (see Sect. 3.1.2. and 3.1.3.).
313 The green blocks relate to the estimation of irrigation water requirements (IWR) used only by
314 Model C. This involves several phenological models to capture the main dynamics of crop
315 water needs over each growing season (Sect. 3.1.4.) and a moisture-accounting store
316 representing the valley soils (Sect. 3.1.3.). Net irrigation water-use at the catchment scale is
317 computed as a function of IWR, irrigated areas and water availability (i.e. natural streamflow)
318 (Sect. 3.1.3.). The whole modeling chain is fed by precipitation and temperature data.

319 We also stress that smoothing functions were used throughout this framework to remove
320 all threshold nonlinearities from the models’ equations (insofar as possible), as recommended
321 by several authors [e.g. Fenicia et al., 2011]. These smoothing functions will not be shown in
322 the following sections for the sake of clarity.

323

324 **3.1.1. Simplifying assumptions**

325

326 The modeling framework described in Fig. 2 relies on three important assumptions regarding
327 the representation of IWU and IWR at the catchment scale:

328

329 (1) First, IWU refers to the amount of water lost by evapotranspiration from the cropped
330 fields and the riparian vegetation that thrives along the irrigation canals. It should not
331 be confused with the actual surface-water withdrawals (SWW) that vary on a weekly
332 or monthly basis depending on historical water rights and planning/management
333 decisions. SWW include IWU but also non-consumptive losses caused by canal
334 seepage and deep percolation in the fields. Unfortunately, the impact of SWW on the
335 catchment behavior is difficult to estimate because reliable information on these

336 additional losses and the proportion of abstracted flows coming back to the system is
337 lacking. In this study, all return flows were assumed to come back to the river within
338 each 10-day time step. A similar assumption can be found in Kiptala et al. [2014].
339

340 (2) Second, IWR refer to the amount of water needed to satisfy crop evapotranspiration
341 under optimal conditions. In practice, this quantity depends on the irrigation technique
342 used by the farmers. In furrow-irrigated fields, IWR would be expected to bring the
343 soil moisture to saturation (or field capacity) and thereby satisfy crop water needs
344 during several days. In drip-irrigated fields, irrigation is required to compensate for the
345 difference between the amount of water stored in the soil and crop water needs. In this
346 study, we assumed that both irrigation techniques lead to the same water requirements
347 over a sufficiently long time interval.
348

349 (3) Third, the two varieties (Flame Seedless, Moscatel Rosada) selected to represent
350 phenological patterns in the valleys are at best a rough approximation of the real crop
351 diversity in this catchment. In reality, phenological dates for each type of grape (pisco
352 or table grapes) can spread over several days or weeks depending on the variety
353 involved. For instance, pisco producers report differences of between 1 and 2 weeks
354 between the various varieties used for pisco [Ibacache et al., 2010].
355

356 Taking heed of these underlying assumptions, all Models (A, B and C) were run at a daily
357 time step but evaluated using a 10-day time step. This 10-day interval was also more
358 consistent with the temperature-index approach used to estimate snowmelt rates [Hock, 2003]
359 (Sect. 3.1.2.).
360

361 **3.1.2. Snow accumulation and ablation modules**

362

363 The snow accumulation and ablation (SAA) modules developed in this study borrow much of
364 their philosophy and equations from the Cemaneige model [Valéry et al., 2014]. The
365 catchment was divided into 5 elevation zones (EZ) of equal area, within which separate
366 modules operated simultaneously based on the same set of parameters. At each time step t ,
367 precipitation was partitioned into rain and snow by assuming a linear transition from snow to
368 rain across a fixed temperature range defined as $[-1^{\circ}\text{C}, 3^{\circ}\text{C}]$ [L'Hôte et al., 2005]. The

369 amount of water contained in the snowpack, or Snow Water Equivalent (SWE, in mm), was
 370 then updated as:

$$SWE_t = SWE_{t-1} + Snow_t \quad (1)$$

371 As in the original Cemanige model, an antecedent temperature index approach was used to
 372 keep track of the snowpack temperature (T_S , in °C) and determine when the pack was ready to
 373 melt:

$$T_{S,t} = \min[0, \theta_S T_{S,t-1} + (1 - \theta_S) T_{A,t}] \quad (2)$$

374 where T_A (°C) is the mean air temperature within the elevation zone and θ_S is a parameter
 375 quantifying the sensitivity of the snowpack temperature to T_A . As such, θ_S is expected to be
 376 higher in regions characterized by thick snowpacks (see also Sect. 4.2.1.). A similar
 377 representation can be found in other hydrological models, including enhanced versions of
 378 SWAT [Fontaine et al., 2002] and SRM [Harshburger et al., 2010]. ~~In general, θ_S is expected~~
 379 ~~to increase with the thickness of the snowpack (see also Sect. 4.2.1.).~~ Melt rates (mm day⁻¹)
 380 were computed as follows:

$$Melt = \begin{cases} \min[SWE, MF(T_A - T_{thr}) + Y_N / (\rho \lambda_f)] \times f(F_{SCA}) & \text{if } T_S = 0^\circ\text{C} \text{ and } T_A \geq T_{thr} \\ 0 & \text{if } T_S < 0^\circ\text{C} \text{ or } T_A < T_{thr} \end{cases} \quad (3)$$

$$\text{with } Y_N = \begin{cases} -C_T \times SWE \times \Delta T_S & \text{for Model A} \\ \Delta R_{SW} + \Delta R_{LW} - C_T \times SWE \times \Delta T_S & \text{for Models B and C} \end{cases} \quad (4)$$

$$f(F_{SCA}) = (1 - V_{min})F_{SCA} + V_{min} \quad (5)$$

$$F_{SCA} = \min[1, SWE/SWE_{max}] \quad (6)$$

381 where MF (mm °C⁻¹ day⁻¹) is the melt factor, T_{thr} is the temperature threshold at which
 382 snowmelt begins (usually set at 0°C), λ_f is the latent heat of fusion (~0.34 MJ kg⁻¹ at 0°C), ρ is
 383 the density of water (~1000 kg m⁻³), ΔR_{SW} and ΔR_{LW} (MJ m⁻² day⁻¹) are the net shortwave and
 384 longwave radiations respectively (more details are given in the Appendix), C_T is the specific

385 heat of snow ($\sim 0.0021 \text{ MJ kg}^{-1}$ at 0°C), F_{SCA} is the fractional snow-covered area and V_{min} is a
 386 parameter accounting for the effects of low SWE levels on melt rates. Y_{N} represents the
 387 energy available from net radiation and changes in the snowpack heat storage. The F_{SCA}
 388 function can be thought of as a basic depletion curve representing the influence of snow
 389 distribution within each zone. As a first approximation, it was assumed to increase linearly
 390 with SWE until a threshold SWE_{max} was reached, above which the whole elevation zone was
 391 assumed to be covered by snow. Following Valéry et al. [2014], the value of SWE_{max} was
 392 fixed at 90% of the mean annual snowfall observed within each elevation zone separately.
 393 Similarly, the value of V_{min} was fixed at 0.1 as in the original Cemaneige model [Valéry et al.,
 394 2010b] to ensure that melt still occurred when F_{SCA} was close to zero. ~~Net shortwave and
 395 longwave radiations were computed as follows:~~

$$\Delta R_{\text{SW}} = (1 - \alpha)\tau R_{\text{e}} \quad (7)$$

$$\Delta R_{\text{LW}} = \epsilon_{\text{A}}\sigma(T_{\text{A}} + 273.15)^4 - \epsilon_{\text{S}}\sigma(T_{\text{S}} + 273.15)^4 \quad (8)$$

396 ~~where α is the snow albedo, τ is the atmospheric transmissivity, R_{e} is the extraterrestrial
 397 radiation ($\text{MJ m}^{-2} \text{ day}^{-1}$) calculated from the latitude and the Julian day [Allen et al., 1998], σ
 398 is the Stefan-Boltzmann constant ($4.89 \cdot 10^{-15} \text{ MJ m}^{-2} \text{ K}^{-4}$), ϵ_{S} is the longwave emissivity for
 399 snow (0.97) and ϵ_{A} is the atmospheric longwave emissivity estimated as in Walter et al.
 400 [2005]. Snow albedo generally decreases between snowfalls as a result of metamorphic
 401 processes. This was represented in the model by adjusting an exponential decay rate related to
 402 the number of days since the last snowfall (N_{t}):~~

$$\alpha_{\text{t}} = \alpha_{\text{min}} + (\alpha_{\text{max}} - \alpha_{\text{min}})e^{-k_{\text{a}}N_{\text{t}}} \quad (9)$$

403 ~~where α_{min} and α_{max} are the minimum and maximum snow albedos, and k_{a} is a recession
 404 factor. These parameters were determined from the literature [Lhermitte et al., 2014;
 405 Abermann et al., 2014] to prevent over fitting (see Table 1). For shallow snowpacks such as
 406 those found around 30°S , albedo values also decrease during snowmelt periods as the
 407 influence of the underlying ground increases. This can have significant effects on melt rates,
 408 which were accounted for implicitly through the V_{min} parameter in Eq. (5). Based on radiation
 409 data available over the last few years (not shown here), atmospheric transmissivity was set at~~

410 | ~~0.75 under clear sky conditions (precipitation < 5 mm) and 0.4 on cloudy days (precipitation~~
 411 | ~~≥ 5 mm).~~ For Models B and C, sublimation losses (mm day⁻¹) were estimated as follows:

$$\text{Sublimation} = \begin{cases} 0 & \text{if } T_A \geq T_{\text{thr}} \\ \min[\text{SWE}, Y_N/(\rho\lambda_s)] \times f(F_{\text{SCA}}) & \text{if } T_A < T_{\text{thr}} \end{cases} \quad (407)$$

412 | where λ_s is the latent heat of sublimation ($\sim 2.84 \text{ MJ kg}^{-1}$ at 0°C). Note that when $T_A \geq T_{\text{thr}}$ and
 413 | $T_s < 0^\circ\text{C}$, all the energy available at the snow surface was used to warm the snowpack. The
 414 | SAA module of Model A is equivalent to the Cemaneige model [Valéry et al., 2014] whereas
 415 | that of Models B and C corresponds to an enhanced version of this model in which
 416 | sublimation and net radiation are considered explicitly. However, both of these modules rely
 417 | on the same calibrated parameters.

418 |

419 | 3.1.3. Runoff production and routing modules

420 |

421 | Spatially-averaged rainfall and snowmelt estimates were combined into a single
 422 | ‘precipitation’ term that was used as input to the lumped GR4J model [Perrin et al., 2003].
 423 | Potential evapotranspiration (PE) was first determined for each grid cell using the
 424 | temperature-based formula proposed by Oudin et al. [2005]:

$$\text{PE}_{\text{Oudin,C}} = \begin{cases} R_e(T_{A,C} + K_2)/(\rho\lambda_v K_1) & \text{if } T_A + K_2 > 0 \\ 0 & \text{otherwise} \end{cases} \quad (418)$$

425 | where $T_{A,C}$ ($^\circ\text{C}$) is the interpolated air temperature of cell C, λ_v is the latent heat of
 426 | vaporization ($\sim 2.46 \text{ MJ kg}^{-1}$) and K_1 (5°C) and K_2 (100°C) are fitted parameters (see Sect.
 427 | 3.1.4. for further details). Spatially-averaged PE inputs to the GR4J model (i.e. PE_{GR4J}) were
 428 | obtained after subtracting the energy consumed by melting and sublimation:

$$\text{PE}_{\text{GR4J}} = \max\left(\sum_C \text{PE}_{\text{Oudin,C}}/N_C - \sum_Z (\lambda_f \text{Melt}_Z + \lambda_s \text{Sublimation}_Z)/(\lambda_v N_Z), 0\right) \quad (429)$$
~~$$\sum_C \text{PE}_{\text{Oudin,C}}/N_C - \sum_Z (\lambda_f \text{Melt}_Z + \lambda_s \text{Sublimation}_Z)/(\lambda_v N_Z)$$~~

429 | where N_C is the number of grid cells, N_Z is the number of elevations zones (Z), λ_v is the latent
 430 | heat of vaporization ($\sim 2.46 \text{ MJ kg}^{-1}$) and $\text{PE}_{\text{Oudin,C}}$ (mm) is given by Eq. (11). Note that PE_{GR4J}
 431 | accounts for evapotranspiration from soils, natural vegetation and crops only insofar as it

432 relates to precipitation or meltwater. It is not supposed to include evapotranspiration from
 433 cultivated areas caused by irrigation water-use. Thus, the GR4J model simulates only those
 434 hydrological processes that relate to the ‘natural’ catchment behavior. Incorporation of IWU
 435 in the modeling framework does not modify the structure and governing equations of the
 436 GR4J model but only the estimates of natural streamflow. This choice can be justified by the
 437 fact that the cultivated areas concentrate mainly in the lower part of the catchment and
 438 represent only a small portion of the total area (Fig. 1).

439 The GR4J model was chosen for its simplicity and parsimony. Basically, the precipitation-
 440 runoff process is broken down into two components: a runoff generation module computes the
 441 amount of water available for runoff, i.e. ‘effective precipitation’, while a routing module
 442 subsequently routes this quantity to the catchment outlet. In the first module, a soil-moisture
 443 accounting (SMA) store is used to partition the incoming rainfall and/or snowmelt into
 444 storage, evapotranspiration and excess precipitation. At each time step, a fraction of the SMA
 445 store is also computed to represent soil drainage and added to excess precipitation to form the
 446 effective precipitation. The second module splits this quantity between two different pathways
 447 with respect to a constant ratio: 10% passes as direct runoff through a quick flow routing path
 448 based on a unique unit hydrograph whereas 90% passes as delayed runoff through a slow flow
 449 routing path composed of a unit hydrograph and an additional routing store. Outputs from
 450 both pathways are finally added up to simulate natural streamflow at the catchment outlet.
 451 This model relies on four calibrated parameters ($X1$, $X2$, $X3$ and $X4$) that are described in
 452 Table 1.

453

3.1.4. Irrigation water-use module (Model C)

454

455
 456 In Model C, irrigation water requirements per unit area (IWR, in mm day⁻¹) were
 457 estimated for each crop variety i using a simple soil-water balance approach:

$$IWR_i = \max[0, ETM_i - SWC_i - P_{\text{valley}}] \quad (4310)$$

$$\text{with } ETM_i(T_{A,V}) = K_{C,i} ET_0(T_{A,V}) \quad (4411)$$

458 where ETM (mm day⁻¹) refers to crop evapotranspiration under optimal conditions and SWC
 459 (mm) to the average soil-water content in the root zone. P_{valley} (mm day⁻¹), ET_0 (mm day⁻¹)

460 and $T_{A,V}$ ($^{\circ}\text{C}$) are respectively the areal effective precipitation, reference evapotranspiration
 461 and air temperature in the valleys, and K_C is a coefficient depending on crop growth stages. A
 462 realistic estimate of ET_0 was provided by using a modified version of Oudin's formula (Eq.
 463 (11)). In Oudin et al. [2005], the values of K_1 and K_2 were chosen as those giving the best
 464 streamflow simulations for different hydrological models applied to a large number of
 465 catchments. In this study, the FAO Penman-Monteith equation for a reference grass was used
 466 as a basis to re-calibrate these parameters at different locations across the valleys. This
 467 modification was required since the Penman-Monteith equation, which was more suited to
 468 estimating crop water needs, could not be used over the whole study period due to limited
 469 data availability (wind speed, relative humidity, solar radiation). Interpolated K_C curves were
 470 constructed for each crop variety using a series of phenological models to simulate the annual
 471 dates of budburst, full bloom, harvest and leaf fall (see Sect. 3.1.5.). The value of K_C at each
 472 of these dates ($K_{C,BB}$, $K_{C,FB}$, $K_{C,HV}$ and $K_{C,LF}$) was determined from the literature [Villagra et
 473 al., 2014] and interviews with local grape growers. Net irrigation water-use in the catchment
 474 (IWU, in $\text{m}^3 \cdot \text{s}^{-1}$) was computed as a function of IWR, irrigated areas and surface-water
 475 availability:

$$| \text{IWU} = \begin{cases} \min \left[Q_{\text{nat}} - Q_{\text{min}}, \sum_i \text{IWR}_i \times A_i / \epsilon \right] & \text{if } Q_{\text{nat}} \geq Q_{\text{min}} \\ 0 & \text{otherwise} \end{cases} \quad (4512)$$

476 where Q_{nat} ($\text{m}^3 \text{ s}^{-1}$) is the natural streamflow simulated by the GR4J model, ϵ is a conversion
 477 factor and A_i (ha) is the irrigated area for crop variety i , which varies on a yearly basis as
 478 shown in Fig. 1b. Q_{min} ($\text{m}^3 \text{ s}^{-1}$) is a minimum discharge below which no withdrawal is
 479 allowed. This parameter was fixed at $0.25 \text{ m}^3 \text{ s}^{-1}$ based on historical low-flow records.
 480 Simulated (influenced) discharge at the catchment outlet was computed from the difference
 481 between Q_{nat} and IWU at each time step. When IWR could not be entirely satisfied, irrigation
 482 water was allocated to each crop variety i in proportion to its irrigated area:

$$| \text{AIW}_i = \min \left[\text{IWR}_i, \epsilon \times \text{IWU} \times A_i / A_{\text{tot}} \right] \quad (4613)$$

483 where AIW_i (mm) is the amount of water allocated to crop variety i and A_{tot} (ha) is the sum of
 484 all irrigated areas. Finally, the average soil water-content in the root zone was updated as:

$$SWC_{i,t} = \max[0, SWC_{i,t-1} + P_{\text{Valley},t} + AIW_{i,t} - ETM_{i,t}] \quad (4714)$$

485

486

487 **3.1.5. Phenological modeling (Model C)**

488

489 To construct the K_C curves, the growing season was split into five phenophases:
 490 endodormancy, ecodormancy, flowering, ripening and senescence. For each grapevine
 491 variety, different process-based models were applied to predict the start and end dates of each
 492 phenophase (Fig. 3).

493 A simplified version of the UniChill model [Chuine, 2000] was chosen to simulate the
 494 annual dates of budburst (t_{BB}). This model covers the periods of endodormancy, when growth
 495 inhibition is due to internal physiological factors, and ecodormancy (or quiescence), when
 496 buds remain dormant because of inadequate environmental conditions. To emerge from
 497 endodormancy, grapevines usually require an extended period of low temperatures, which is
 498 represented in the model as an accumulation of ‘chilling’ rates R_{CH} :

$$C_{BB} = \sum_{t=t_0}^{t_1} R_{CH}(T_{A,V}) \quad (4815)$$

$$R_{CH}(T_{A,V}) = 1/\left[\delta \left(1 + e^{a(T_{A,V}-b)^2}\right)\right] \quad (4916)$$

499 where $T_{A,V}$ is the average daily temperature in the valley and t_0 , a , b and C_{BB} are fitted
 500 parameters described in Table 1. δ is a scaling factor set at 0.5 to ensure that the optimal
 501 chilling rate (when $T_{A,V} = b$) has a value of 1 [Caffarra and Eccel, 2010]. A sensitivity analysis
 502 (not shown here for brevity’s sake) was performed to determine the optimal value for t_0 , i.e.
 503 the starting date of the endodormancy period (see Table 1). Likewise, from dormancy release
 504 to budburst an extended period of high temperatures is generally required (ecodormancy).
 505 This process is represented as an accumulation of ‘forcing’ rates R_{BB} :

$$F_{\text{BB}} = \sum_{t=t_1}^{t_{\text{BB}}} R_{\text{BB}}(T_{\text{A,V}}) \quad (2017)$$

$$R_{\text{BB}}(T_{\text{A,V}}) = 1/[1 + e^{c(T_{\text{A,V}}-d)}] \quad (218)$$

506 where c , d and F_{BB} are fitted parameters. To prevent over-parameterization, the values of c
 507 and d were fixed at -0.25 and 15°C based on information available in the literature [Caffarra
 508 and Eccel, 2010; Fila et al., 2012]. The sigmoid function of Eq. (21) describes the temperature
 509 dependence of growth rates in a more realistic way than usual approaches based on growing
 510 degree-days.

511 The 4-parameter model developed by Wang and Engel [1998] (hereafter referred to as
 512 WE) was selected to simulate the annual dates of full bloom (t_{FB}) and harvest (t_{HV}):

$$F_{\text{FB}} = \sum_{t=t_{\text{BB}}}^{t_{\text{FB}}} R_{\text{FB}}(T_{\text{A,V}}) \quad \text{and} \quad F_{\text{HV}} = \sum_{t=t_{\text{FB}}}^{t_{\text{HV}}} R_{\text{HV}}(T_{\text{A,V}}) \quad (219)$$

$$R_{\text{FB}}(T_{\text{A,V}}) = R_{\text{HV}}(T) \quad (220)$$

$$= \begin{cases} \frac{2(T_{\text{A,V}} - T_{\text{min}})^\alpha (T_{\text{opt}} - T_{\text{min}})^\alpha - (T_{\text{A,V}} - T_{\text{min}})^{2\alpha}}{(T_{\text{opt}} - T_{\text{min}})^{2\alpha}} & \text{if } T_{\text{min}} \leq T_{\text{A,V}} \leq T_{\text{max}} \\ 0 & \text{otherwise} \end{cases}$$

$$\text{with } \alpha = \log(2)/\log[(T_{\text{max}} - T_{\text{min}})/(T_{\text{opt}} - T_{\text{min}})] \quad (221)$$

513 where F_{FB} , F_{HV} and T_{opt} ($^\circ\text{C}$) were calibrated separately for each variety. Note that T_{opt} also
 514 varies with the phenophase under study (flowering or ripening). Compared to other flowering
 515 and harvest models based on forcing rates, this one has the major advantage of also
 516 accounting for the inhibiting effect of extreme temperatures on photosynthesis. As leaf growth
 517 typically ceases at temperatures below $0\text{--}5^\circ\text{C}$ [Hendrickson et al., 2004] and above $35\text{--}40^\circ\text{C}$
 518 [Greer and Weedon, 2013], parameters T_{min} and T_{max} were fixed beforehand at 0°C and 40°C
 519 respectively [García de Cortázar-Atauri et al., 2010].

520 Eventually, the post-harvest period was modeled as a constant number of days (N_{LF})
 521 between t_{HV} and the end of leaf fall (t_{LF}). The value of N_{LF} was obtained from interviews with
 522 local grape growers for each variety (see Table 1).

523

524 **3.2. Model evaluation**

525

526 The phenological and hydrological models were evaluated separately using different methods
527 and/or objective functions. Models A and B have the same number of calibrated hydrological
528 parameters (i.e. 6 parameters).

529

530

531

532 **3.2.1. Hydrological modeling**

533

534 The dataset was divided into a calibration period (1985–1995), showing a sharp increase in
535 irrigated areas (+100%), and a validation period (1995–2005), characterized by a much lower
536 increase (+20%) (Fig. 1b). Each period was defined in terms of water years (from May 1 to
537 April 30) and included at least one major El Niño (1987–88, 1997–98 and 2002–03) or La
538 Niña (1988–89, 1998–99 and 1999–00) event.

539 The models were evaluated using either (1) simulations obtained with a single, ‘optimal’
540 parameter set, or (2) probabilistic predictions obtained by sampling the posterior distributions
541 of the parameters. In the first case, model efficiency and internal consistency were assessed.
542 In the second case, predictive uncertainty bands were derived and scrutinized in terms of
543 reliability and sharpness.

544

545 ***Model efficiency and internal consistency***

546 Model efficiency measures the ability to fit the observed behavior of the system with regard to
547 specific criteria. In this study, the Shuffle Complex Evolution (SCE) algorithm [Duan et al.,
548 1993] was used to maximize the following criterion:

$$F_{\text{obj}} = (KGE + KGE_{\text{inv}})/2 \quad (2522)$$

549 where KGE and KGE_{inv} refer to the Kling-Gupta Efficiency [Gupta et al., 2009] computed
550 from discharge (Q) and inverse discharge (1/Q) values respectively. This composite criterion
551 was chosen to emphasize high and low flows equally [Pushpalatha et al., 2012; Nicolle et al.,
552 2014].

553 Internal consistency can be defined as the ability to reproduce the dynamics of internal
554 catchment states without conditioning the model parameters on additional data. Here, this
555 analysis was limited to the Snow Accumulation and Ablation module to evaluate its ability to
556 reproduce the seasonal pattern of snow storage and release within each elevation zone. This
557 was achieved through visual inspection of model-based and MODIS-derived F_{SCA} time series
558 and based on the snow error criterion defined in Hublart et al. [2015].

559

560

561

562 *Model predictive uncertainty*

563 The Differential Evolution Adaptive Metropolis (DREAM) algorithm [Vrugt et al., 2009] was
564 chosen to approximate the posterior distributions of model parameters and obtain probabilistic
565 streamflow predictions. This required a statistical model of the differences between observed
566 and simulated flows (i.e. residual errors). We used the Generalized Likelihood (GL) function
567 introduced by Schoups and Vrugt [2010], which describes correlated, heteroscedastic and
568 non-gaussian errors based on a number of parameters given in Table 1. Uniform priors were
569 assumed to reflect the lack of information on model parameters in this catchment. ~~Acceptance~~
570 ~~rates during the MCMC sampling procedure were maintained between 20 and 30% by tuning~~
571 ~~the scale of the second proposal in the DREAM algorithm.~~ After a maximum of 30,000
572 iterations, the quantitative diagnostic of Gelman and Rubin [1992] was used to determine
573 when the chains had converged to the stationary posterior distribution.

574 The reliability of the predictive distributions was first assessed by checking for the ability
575 of various p -confidence intervals (with $p = 0.05$ to 0.95) to bracket the adequate percentage of
576 streamflow observations (hereafter called POCI for Percentage of Observations within the p -
577 Confidence Interval):

$$POCI(p) = N(Q_{obs} \in [Limit_{Upper}(p), Limit_{Lower}(p)] \forall t) / n \quad (2623)$$

578 where n is the total number of observations, $Limit_{Upper}(p)$ and $Limit_{Lower}(p)$ are the upper and
579 lower boundary values of the p -confidence interval and N indicates the number of
580 observations enclosed within these boundaries. When plotted as a function of p , the POCI
581 points should fall along the diagonal 1:1 line. The predictive distributions were also verified
582 using the Probability Integral Transform (PIT) values of streamflow observations, defined as
583 [e.g. Thyer et al., 2009; Wang et al., 2009; Engeland et al., 2010]:

$$\pi_t = F_t(Q_{\text{obs},t}) \quad (2724)$$

584 where F_t is the empirical cumulative distribution function (CDF) of streamflow predictions at
 585 time t . For ideal predictions (i.e. based on correct statistical assumptions regarding model
 586 errors), the π_t values are expected to be uniformly distributed between 0 and 1. More details
 587 on the correct use and interpretation of PIT plots, including the use of Kolmogorov
 588 significance bands as a test of uniformity, can be found in Laio and Tamea [2007] (see also
 589 Fig. 4).

590 Finally, the sharpness (or ‘resolution’) of the predictive distributions was measured using
 591 the Average Relative Interval Length (ARIL) criterion proposed by Jin et al. [2010], which
 592 should be as small as possible for any p between 0 and 100%:

$$\text{ARIL}(p) = \frac{1}{n} \sum_t [\text{Limit}_{\text{Upper},t}(p) - \text{Limit}_{\text{Lower},t}(p)] / Q_{\text{obs},t} \quad (2825)$$

593 Each of these posterior diagnostics (POCI, PIT and ARIL) was performed separately for all
 594 streamflow observations and three distinct regions of the observed flow duration curve,
 595 namely: high-flows (20% exceedance probability), mid-flows (20 to 80% exceedance
 596 probability) and low-flows (20% exceedance probability).

598 3.2.2. Phenological modeling

599
 600 The phenological models used in Model C were calibrated by minimizing the root-mean-
 601 square error (RMSE) between simulated and observed phenological dates over the whole
 602 dataset (2003–2013). This was achieved using the SCE algorithm with the same number of
 603 complexes for all models and crop varieties. Given the small number of available
 604 observations, a leave-one-out cross-validation technique was chosen to assess the robustness
 605 of each model. Additional metrics such as the Nash-Sutcliffe Efficiency (NSE) and the mean
 606 difference between observed and predicted dates (i.e. model bias) were also used in validation
 607 to characterize the modeling errors. On the whole, 8 parameters required calibration for each
 608 variety (Table 1).

609
 610

611 **4. Results**

612

613 **4.1. Phenological simulations**

614

615 Figure 5, Table 2 and Table 3 show the results obtained for both grapevine varieties with the
616 three phenological models. On the whole, approximately 76% of the differences between
617 observed and predicted phenological dates fell within the range of ± 5 days during
618 calibration (Fig. 5). Moreover, mean absolute errors did not exceed 6.4 days in any case. Such
619 errors can be considered acceptable with regard to the 10-day time step chosen to evaluate the
620 hydrological models.

621 The best results were obtained for Flame Seedless with the budburst (BB) model and for
622 Moscatel Rosada with the full bloom (FB) and harvest (HV) models. RMSE values ranged
623 from 3.0 to 6.1 days in calibration and from 5.4 to 7.9 days in validation, indicating a
624 moderate loss of performance (Table 2). In general, bias values remained close to zero, except
625 for Moscatel Rosada with the HV model. NSE values were positive for all varieties and
626 models in calibration but decreased sharply in validation, with only two values above 0.50
627 and one negative value for Flame Seedless with the FB model. However, very low to negative
628 NSE values are not uncommon in phenological modeling when only a few observations (< 10
629 years) collected from a single site are used to calibrate the models [e.g. Parker et al., 2013].
630 The optimized parameter values displayed in Table 3 are discussed in Sect. 5.4.

631

632 **4.2. Hydrological simulations**

633

634 **4.2.1. Model efficiency and internal consistency**

635

636 Table 4 show the results obtained from the calibration and validation of Models A, B and C.
637 Clearly, Model C was found to perform better than Models A and B with respect to the
638 objective function given by Eq. (25). This higher performance was mostly the result of
639 improved low-flow simulations (KGE_{inv}). Table 5 shows that simulated sublimation rates and
640 contribution to snow ablation remained approximately the same when IWU was introduced in
641 the model equations. Estimated mean annual sublimation rates at high elevations (EZ no. 4
642 and 5) were consistent with those found by other studies, including experimental studies
643 conducted on small glaciers of the region [MacDonell et al., 2013].

644 The internal consistency of the SAA module was verified over an independent validation
645 period (2000–2011) using the parameters (θ_s , MF) calibrated with each Model from 1985 to
646 1995. The snow errors displayed in Table 4 vary from 2% in the first elevation zone (EZ no.
647 1) to 11–17% in the last one (EZ no. 5). Such errors were very encouraging, as they were
648 comparable to those obtained by Hublart et al. (2015) in the same catchment with less
649 parsimonious (and less realistic) snowmelt models. The impact of considering net radiation
650 and sublimation in the model equations, however, was only evident for EZ no. 4 and 5, where
651 a moderate drop in the snow error was observed. Model A even performed slightly better than
652 Model B with respect to the F_{obj} function, ~~showing that (supposedly) improved internal~~
653 ~~consistency (and model realism) may not necessarily go with improved model performance~~
654 ~~when looking at the system's integrated response (i.e. streamflow).~~

655 Figure 6 provides a visual comparison of simulated and observed fractional snow-covered
656 areas (F_{SCA}) during this validation period for Model C. On the whole, it can be seen that the
657 SAA model did not accumulate snow from one year to another, which was consistent with the
658 observed inter-annual pattern of snow cover in the catchment. However, there were important
659 discrepancies between the lower and upper elevation zones. In the lower zones (EZ no. 2 and
660 3), the model did fairly well during several years of the period (e.g. 2001, 2004, 2009 and
661 2010) but also under-estimated the annual snow cover duration (SCD) during several other
662 years (e.g. 2002, 2003 and 2007). In the upper zones (EZ no. 4 and 5), the model generally
663 failed to reproduce the observed variations in F_{SCA} despite improved estimates of the annual
664 SCD. In EZ no. 5, there was also a tendency to over-estimate the SCD during the last 3–4
665 years of the period.

666

667 **4.2.2. Model predictive uncertainty**

668

669 Between 10 000 and 13 000 model evaluations were required to reach convergence to a
670 limiting distribution depending on the Model used. In each case, the last 5 000 samples
671 generated with DREAM were used to compute the posterior diagnostics presented in Sect.
672 3.2.1. and generate predictive uncertainty bands.

673

674 Figure 7 provides a range of formal tests of the statistical assumptions made to describe
675 model residuals in the case of Model C. The density plot of Fig. 7a confirms that model
676 residuals were broadly symmetric and kurtotic, although kurtosis appears to be slightly
677 overestimated. Heteroscedasticity (Fig. 7c) was largely removed by the variance model of the

678 GL function. However, Fig. 7b shows that the assumption of independence was not fully
679 respected, as residuals remained slightly correlated (0.35) at a lag of 1 and at some greater
680 lags, indicating potential storage errors in the model structure.

681
682 Figure 8 displays the scatter plots and posterior histograms of hydrological parameters for
683 Models A and C. The results obtained with Model B are not shown here as they were
684 generally close to those of Model C. As can be seen, differences between the structures of
685 Models A and C had no particular effect on parameter identifiability. All parameters appeared
686 to be relatively well-defined with approximately Gaussian distributions, although the values
687 of θ_s , MF and $X3$ occupied a wider range of their prior intervals with Model A than with
688 Models B and C. Introducing sublimation and net radiation in the SAA module reduced the
689 correlation between θ_s and MF observed with Model A but simultaneously increased the
690 interaction of θ_s with $X3$ and $X4$. Likewise, additional checks performed with Models B and C
691 showed that the incorporation of irrigation water-use in Model C led to a strong correlation
692 between $X2$ and $X3$, which questions the internal consistency of the Runoff production and
693 routing module when increasing the model complexity. ~~with Models B and C showed that the~~
694 ~~strong correlation between $X2$ and $X3$ observed for Model C was mainly due to the~~
695 ~~incorporation of irrigation water use in the modeling framework.~~

696
697 Figure 9 shows the posterior diagnostics used to evaluate the reliability (PIT, POCI) and
698 resolution (ARIL) of forecast distributions for Models B and C. At first sight, the PIT values
699 obtained with all streamflow observations appear to be distributed quite uniformly during
700 both simulation periods. Small departures from the diagonal line and the 5% Kolmogorov
701 confidence bands indicate a tendency to under-predict the observed data, but this applies to
702 both models, especially in validation. On the contrary, significant differences between the two
703 models become obvious when looking at specific portions of the observed flow duration
704 curve. At low flows, the PIT values obtained with Model B revealed a significant over-
705 prediction bias during both calibration and validation periods. While it did not affect the
706 percentage of observations covered by the confidence intervals (as POCI values remained
707 close to the diagonal line), this systematic bias resulted in very high ARIL values (exceeding
708 1.5 in calibration and 3 in validation with the 95% confidence intervals). By contrast, Model
709 C slightly over-estimated predictive uncertainty in calibration but led to highly reliable low-
710 flow predictions in validation, as evidenced by the PIT and POCI plots. This resulted in
711 relatively low ARIL values (< 1). At mid-flows, the two models exhibited a similar behavior

712 characterized by a systematic under-prediction bias, under-estimated POCI values and
713 relatively low ARIL values (< 1). At high flows, the PIT values were well within the
714 Kolmogorov confidence bands for both models, although there was still a tendency to under-
715 predict the observed data. In validation, this under-prediction bias translated into an
716 excessively low number of observations enclosed within any p -confidence interval for $p >$
717 70%.

718

719 Figure 10 shows the uncertainty bands obtained with Models B and C during the two
720 simulation periods. The dark blue region represents the uncertainty in streamflow predictions
721 associated with the posterior parameter distributions while the light blue region represents the
722 total uncertainty arising from parameter, model structure and input errors simultaneously.
723 Some portions of the observed hydrograph have been enlarged to highlight key differences
724 between the two models. In general, uncertainty bands should be wide enough to include the
725 expected percentage of streamflow observations (here, 95%), but not so wide that the
726 representation of the observed hydrograph becomes meaningless. From this perspective, the
727 main differences between Models B and C were observed for summer flows, i.e. during the
728 irrigation season. Model B results in large uncertainty bands that are able to capture most of
729 the observations but which fail to reproduce the seasonal pattern of streamflow during dry
730 years (e.g. 1989–90, 1994–95, 1996–97, 1997–98, 1999–00). In this case, structural and input
731 errors represent the dominant sources of uncertainty. By contrast, the width of the prediction
732 limits obtained with Model C tends to decrease as the magnitude of the predicted streamflow
733 decreases. In this case, parameter uncertainty accounts for most of the predictive uncertainty
734 during summer. However, winter and early summer flows are often under-predicted by both
735 models. This last point is further discussed in Sect. 5.3.

736

737

738 5. Discussion

739

740 5.1. Summary

741

742 ~~This paper investigated the reliability of a parsimonious precipitation-runoff model in a~~
743 ~~subtropical mountainous catchment where irrigated areas have increased significantly over the~~
744 ~~past 30 years. More specifically, it explored the usefulness of explicitly accounting for snow~~

745 ~~sublimation and irrigation water use (IWU) in conceptual modeling frameworks operating at~~
746 ~~the catchment scale. To this end, a 20-year simulation period (1985–05) encompassing a wide~~
747 ~~range of climate and water use conditions was selected to evaluate three types of integrated~~
748 ~~Models referred to as A, B and C. These Models relied on the same runoff generation and~~
749 ~~routing module, i.e. the GR4J model, but differed in their underlying assumptions and~~
750 ~~governing equations regarding snowmelt and IWU effects. The introduction of sublimation~~
751 ~~helped to reduce errors in the simulation of fractional snow covered areas at high elevations.~~
752 ~~At low flows, the reliability of probabilistic streamflow predictions was greatly improved~~
753 ~~when IWU was explicitly considered (i.e. with Model C), resulting in relatively narrow~~
754 ~~uncertainty bands and reduced structural errors. This model based analysis provided some~~
755 ~~evidence that water abstractions from the unregulated Claro River is impacting on the~~
756 ~~hydrological response of the system.~~

757 ~~One of the main advantages of this approach is that it provides an estimate of natural~~
758 ~~streamflow which can be used to assess the capacity of the system to meet increasing~~
759 ~~irrigation water needs [e.g. Fabre et al., 2015b]. Another advantage in the context of climate~~
760 ~~change impact studies lies in the use of phenological models based on functions that integrate~~
761 ~~both the negative and positive effects of higher temperatures on crop development. In the~~
762 ~~future, possible feedbacks between the hydrological and crop patterns can be easily added to~~
763 ~~the modeling framework. For instance, variations in irrigated areas could be parameterized as~~
764 ~~a function of water demand satisfaction. Increased satisfaction rates would lead to increased~~
765 ~~irrigated areas, which, in turn, would lead to decreased satisfaction rates, etc. However,~~
766 ~~critical challenges remain to be addressed before the model can be used for such co-~~
767 ~~evolutionary prospective studies.~~

769 **5.2.5.1. Snow accumulation and ablation**

770
771 The ‘optimal’ cold-content factor (θ_s) was very close to 1 with all Models (Fig. 7),
772 indicating a relative insensitivity of the snowpack temperature to changes in air temperature.
773 ~~This runs counterintuitive to finding seems a contradiction of~~ the idea that shallow snow
774 packs such as those observed in the region should have a low thermal inertia. By comparison,
775 Stehr et al. [2009] obtained a value of zero for θ_s after calibrating the SWAT model in a
776 snowmelt-fed catchment of the more humid Central Chile (38°S). One possible explanation
777 for this apparent contradiction is that mean daily temperatures in North-Central Chile are
778 rarely negative at low and mid-elevations (< 4000 m a.s.l.). A high value of θ_s was therefore

779 required to preserve the seasonality of melting during the spring and summer months, despite
780 small snow depths and frequently positive air temperatures throughout the winter. In EZ no. 3
781 and 4, this model requirement may be due to the impact of latent heat fluxes on the snowpack
782 cold-content. During the winter, almost all the energy available from net radiation and
783 sensible heat transfers is consumed by sublimation. This maintains the snowpack temperature
784 slightly below 0°C and effectively delays snowmelt until the mean daily air temperature
785 stabilizes above 0°C for a sufficiently long period of time. Another possible explanation is
786 that a high value of θ_s implicitly accounts for the effect of night-time freezing, which further
787 delays snowmelt despite warm day-time temperatures. At high elevations (> 4000 m a.s.l., i.e.
788 EZ no. 5), where observed air temperatures are mostly negative, we note that a constant lapse
789 rate of 6.0°C km⁻¹, as applied in this study for all elevation zones, was also likely to over-
790 estimate temperature inputs. Lapse rates at these elevations are generally much greater than
791 that, being in fact closer to the dry adiabatic lapse rate. Again, this would be expected to
792 generate high values of θ_s to compensate for temperature over-estimation.

793 The main drawback of this approach (i.e. using air temperature as a proxy for the
794 snowpack cold-content) is that it remains largely implicit and only indirectly connected to the
795 amount of water lost by sublimation in the model (i.e. the outcome of Eq. (10) has no effect
796 on Eq. (2)). This does not mean, however, that a physically-oriented interpretation cannot be
797 sought *a posteriori* to check for the model realism. Alternative approaches can also be used to
798 account for the delay in meltwater production at the start of the ablation season. In general,
799 these will involve an additional store representing the water-holding capacity of the snowpack
800 [Schaepli and Huss, 2011]. Although further research would be required to compare the
801 relative merits of each approach, the representation chosen in this study may be more suited to
802 catchments with shallow snowpacks and significant sublimation.

803 The ‘optimal’ melt factor (MF) was significantly higher with Model A than with Models B
804 and C (Fig. 7). This was not surprising since, in the case of Models B and C, the effects of net
805 radiation were explicitly considered and the melt factor was meant to parameterize only the
806 contribution of turbulent energy fluxes. Such a ‘restricted’ melt factor is expected to increase
807 with increasing wind speed and/or relative humidity, as shown by Brubaker et al. [1996]. The
808 relatively low values ($\sim 2 \text{ mm } ^\circ\text{C}^{-1} \text{ day}^{-1} \text{ mm}^{-1} \text{ day}^{-1}$) obtained here were therefore consistent
809 with the overall dry conditions of the study area. However, we found little evidence of
810 improved model performance and internal consistency when a restricted melt factor was used
811 and net radiation and sublimation were introduced in the model equations (see Table 4). This
812 lack of sensitivity may be due to other sources of uncertainty, in particular regarding the

813 choice of an adequate snow depletion curve to estimate fractional snow-covered areas (Eq.
814 (6)).

815 While most snowmelt routines used in conceptual catchment models assume either
816 entirely snow-free or entirely snow-covered elevation zones, accounting for the proportion of
817 each zone over which snow extends can be critical where mean snow depths are known to be
818 small. As a first approximation, we relied on a linear relationship between SWE and F_{SCA} that
819 did not account for wind redistribution effects or differences in radiation receipt caused by
820 slopes of different aspects. In the dry Andes, wind-induced redistribution has been shown to
821 significantly increase the spatial variability in snow depth, hence reducing the total snow
822 cover area during winter [Gascoin et al., 2013; Ayala et al., 2014]. For a proper assessment of
823 predictive uncertainty, a multi-criteria likelihood function accounting for the differences
824 between several types of simulated and observed responses (typically, fractional snow-
825 covered areas and stream flows) should be used [e.g. Koskela et al., 2012]. This is the subject
826 of ongoing research.

827

828 | **5.3.5.2. Runoff generation and routing**

829

830 Figures 9 and 10 revealed a clear under-prediction bias in the simulation of winter and early
831 spring flows during several water years. Further details on these systematic deficiencies are
832 provided by Fig. 11, which focuses on a specific El Niño event (2002–03). From May to
833 September 2002, the observed winter flow increased rapidly from 0.15 to 0.5 mm day⁻¹ (Fig.
834 11a) in response to intense rainfall events (Fig. 11b) and gradual snowmelt (Fig. 11c). Most of
835 this precipitation, however, served to refill the soil-moisture accounting (SMA) store of the
836 model, which, after three years of intense La Niña-related drought (1999–2002), was only
837 15% of capacity (Fig. 11d). As a result, effective precipitation did not exceed 0.5 mm day⁻¹
838 during this five-month period (Fig. 11e), of which only 10%, i.e. less than 0.05 mm day⁻¹,
839 were processed through the quick flow routing path (Fig. 11f). The remaining 0.45 mm day⁻¹
840 were added to the routing store, whose water level was also very low in May 2012. The
841 overall quantity routed by both pathways was therefore largely insufficient to match the actual
842 streamflow. A similar sequence was observed for all water years characterized by the same
843 failures in streamflow predictions, shedding light on two critical sources of uncertainty [related](#)
844 [to structural deficiencies and input data errors](#).

845

846

5.3.1.5.2.1. Structural deficiencies

Arguably the largest source of structural uncertainty in the hydrological model lies in the representation of runoff production by a single SMA store. This lumps together quite distinct landscape units and misses a number of important differences in the functioning of upland and lowland areas. Of these differences the most notable relate to the terrain over which precipitation occurs. In the mountains, most of the land cover is dominated by barren to sparsely vegetated exposed rocks, boulders and rubble. The topography is steep, with slopes as large as 30° and very poor soil development above the mountain front zone. By contrast, the valley bottoms appear as relatively flat areas largely covered by vegetation. Alluvial fans are also found along the mountain foothills, acting as hydrologic buffers between these two landscape units.

Another key difference arises from the type of precipitation involved. That it occurs mainly as snow in the uplands and rain in the lowlands is expected to have some consequences on the hydrological response of each landscape unit. Snowmelt typically occurs at a much lower and more consistent rate than rainfall, which means that much of the meltwater can be expected to soak into the ground. By contrast, high-intensity rainstorms will tend to exceed the infiltration capacity and increase overland flow. This is especially the case in dryland areas where vegetation cover is sparse and rainfall events highly erratic. Additionally, rainfall events generally occur much closer to the catchment outlet than snowmelt and often not very far from the saturated riparian zone. This limits transmission losses and further enhances overland flow. Rain, while not a dominant feature of semi-arid Andean catchments, can exert a significant influence on winter flows even during dry years. In the GR4J model, as in many other precipitation-runoff models, rainfall and snowmelt inputs are treated as the same kind of 'water' and processed through the same pathways within the model structure. In reality, different types of precipitation will most likely involve different modes of runoff generation. By and large, a greater proportion of rainwater should be expected to bypass the SMA store in comparison to meltwater. This difference remains largely ignored by traditional lumped precipitation-runoff models.

Recent studies have suggested possible ways to make up for these structural deficiencies while preserving the overall simplicity of the lumped conceptual approach [e.g. Savenije et al., 2010; Gharari et al., 2014]. In short, different SMA stores could be used in parallel to represent runoff production from different functional units (i.e. riparian zone, valley bottoms, mountain front, headwaters). The same routing module would then be used to route the

881 ~~overall output from these various production modules. Investigating such modifications was~~
882 ~~far beyond the scope of this study and would greatly benefit from a comparison between~~
883 ~~multiple catchments.~~

884
885 One possible source of model inadequacy lies in the representation of runoff production
886 by a single SMA store, which lumps together quite distinct landscape units. In the mountains,
887 most of the land cover is dominated by barren to sparsely vegetated exposed rocks, boulders
888 and rubble. The topography is steep, with slopes as large as 30° and very poor soil
889 development above the mountain front zone. By contrast, the valley bottoms appear as
890 relatively flat areas largely covered by vegetation. Alluvial fans are also found along the
891 mountain foothills, acting as hydrologic buffers between the mountain blocks and the valleys.

892 Another potential source of structural uncertainty relates to the type of precipitation
893 entering the SMA store. Snowmelt typically occurs at a much lower and more consistent rate
894 than rainfall, and much of the meltwater is expected to soak into the ground. Rain, while not a
895 dominant feature of semi-arid Andean catchments, can exert a significant influence on winter
896 flows even during dry years. While snowmelt events occur mainly in the uplands, most
897 rainfall events take place in the valley bottoms, i.e. much closer to the catchment outlet and
898 generally not very far from the saturated riparian zone. In most precipitation-runoff models,
899 however, rainfall and snowmelt inputs are treated as the same kind of ‘water’ and processed
900 through the same model paths. More research is needed to determine whether different types
901 of precipitation inputs, which would be expected to involve different modes of runoff
902 generation, should translate into different model representations. Investigating such
903 hypotheses was far beyond the scope of this study.

904

905

906 **5.3.2.5.2.2. Impacts of input data errors**

907

908 Relatively high values were obtained for $X1$ (> 1000 mm) and $X2$ ($\sim 4-5$ mm), which was
909 somewhat surprising given our understanding of storage capacities and water fluxes in the
910 Claro River catchment. The $X2$ parameter, in particular, is used to represent groundwater
911 exchanges with the underlying aquifer and/or neighboring catchments. Positive values
912 indicate a net water gain at the catchment scale whereas negative values relate to a net water
913 loss. Le Moine et al. [2007] have shown from the analysis of 1040 French catchments that
914 alluvial aquifers are more likely to be associated with negative values of $X2$ whereas

915 crystalline bedrocks tend to correlate with values centered on zero ($-5 < X2 < 5$). Over the
916 long term, however, the value of $X2$ is expected to be zero if the catchment is a closed system.

917 In this catchment, the valley-fill aquifers that compose most of the groundwater flow
918 system are bounded by large mountain blocks of granitic origin, which drastically limits inter-
919 catchment flow paths. Ground water in the bedrock is typically found in fractures or joints,
920 with a low storage capacity, and soils are, on the whole, poorly developed. As a result, low
921 values of $X1$ and negative values of $X2$ would have seemed more 'realistic'. Note that the
922 autocorrelation structure of model residuals shown in Fig. 7 was also indicative of substantial
923 storage errors in the hydrological model. This lack of physical realism suggests that other
924 factors may be at play. Both of these parameters, indeed, are known to interact strongly with
925 precipitation and evapotranspiration input errors [e.g. Andréassian et al., 2004; Oudin et al.,
926 2006; Thyer et al., 2009]. The capacity of the SMA store tends to increase in the presence of
927 random precipitation errors or if precipitation is systematically over-estimated [Oudin et al.,
928 2006]. Likewise, an excessively high value of $X2$ might indicate that potential
929 evapotranspiration is over-estimated and/or precipitation under-estimated.

930 As in many mountainous catchments, some precipitation events occurring at high
931 elevations may not be captured by the gauging network ($< 3\ 200$ m a.s.l.) used to interpolate
932 precipitation across the catchment. These occasional errors naturally add to systematic
933 volume errors caused by wind, wetting and evaporation losses at the gauge level, leading to an
934 overall underestimation of precipitation at the catchment scale. However, a large uncertainty
935 also surrounds the estimation of elevation effects on precipitation. Mean annual precipitation
936 was assumed to increase by ~ 0.4 m w.e. km^{-1} (Sect. 2.2.1.), yet in the absence of reliable
937 precipitation data above 3 200 m a.s.l., it is unclear whether this gradient under-estimated or
938 over-estimated precipitation enhancement. In general, it is unlikely that a constant value
939 would represent orographic effects correctly at all elevations and over the whole simulation
940 period. Precipitation enhancement in the Andes can vary considerably on a year-to-year basis
941 or from one event to another [Falvey and Garreaud, 2007], leading to time-varying errors in
942 the estimation of precipitation inputs. From Fig. 6 we hypothesize that precipitation was on
943 the whole underestimated, and only occasionally overestimated. Overestimation of potential
944 evapotranspiration is also a plausible hypothesis for Models B and C owing to possible
945 interactions with the estimation of sublimation rates and irrigation water-use (Fig. 7).

946
947
948

5.4.5.3. Phenological modeling

Contrary to lumped catchment models, the phenological models used in this study allow for a direct interpretation of parameter values through comparison with existing experimental studies. This provides a second level of model validation.

The values obtained for T_{opt} (i.e. the optimal forcing temperature) with the full bloom and harvest models (Table 3) were generally close to the range of optimal photosynthetic temperatures reported in the literature, i.e. typically 20–30°C [García de Cortázar-Atauri et al., 2010]. On the contrary, relatively high values (around 11–12°C) were found for parameter b (i.e. the optimal chilling temperature) compared to those reported by previous modeling and experimental [e.g. Fila et al., 2012] studies. Moreover, the values obtained for parameter a , which determines the range of acceptable chilling temperatures around the optimum b , imply that temperatures around 13–16°C were still effective as chilling temperatures. Caffarra and Eccel [2010] and Fila et al. [2014] also found large effective chilling intervals with similar budburst models but different grapevine varieties, which they explained in different ways. In our case, this outcome was most likely related to the use of mean daily temperatures as inputs to the budburst model. Very high diurnal variations (~20°C) can be observed at the INIA experimental site, where a mean temperature of 11–12°C actually reflects temperatures close to 0°C during several hours of the day. The critical states of chilling (C_{BB}) obtained for both varieties indicate that between 11 and 27 days at 11–12°C were required to break endodormancy. Assuming that winter temperatures remained close to zero during at least 5 hours per day, these results are fully consistent with the fact that most grapevine varieties typically require between 50 and 400 hours at temperatures below 7°C to achieve budburst [Fila et al., 2012]. However, given the limited number of years with available observations and the absence of direct evidence for the release of endodormancy, possible trade-offs between the chilling (a , b , C_{BB}) and forcing (F_{BB}) parameters during the optimization process cannot be dismissed *a priori*. Thus, while the phenological models can be considered reliable under the conditions observed over 1985–2005, their results should be treated very carefully when dealing with potential impacts of higher temperatures.

5.5.5.4. Irrigation water-use modeling

While no ground data was available to verify our estimates of irrigation water-use, a comparison was made with net surface-water withdrawals (SWW) estimated from the water access entitlements database (Fig. 12). Not surprisingly, this comparison revealed large discrepancies between these two quantities, especially from 1985 to 1990, which could explain the poor performance of all Models in water years 1985–86 and 1986–87 (Fig. 10). It is worth noting, however, that SWW data reflect more a level of water availability in the catchment than the actual water consumption in the vineyards. These data may also indicate sudden changes in the management of water resources at the regional scale which do not necessarily affect irrigation requirements at the local scale. Overall, the actual water-use in the catchment is likely to be somewhere between simulated IWU and net SWW estimates. Incorporating IWU simulations into conceptual catchment models can help reduce the uncertainty associated with low-flow simulations, yet it is by no means a substitute for accurate measurement of water withdrawals.

The relative stability of simulated IWU from year to year is perhaps more surprising given the complexity of the phenological models used. However, this stability could not be taken for granted before running the models (it can only be observed *a posteriori*). Using phenological models also has considerable advantages in terms of model robustness under climate- and/or human-induced changes, which are further discussed in Section 6.

~~The actual water use in the catchment is likely to be somewhere between simulated IWU and net SWW estimates. Incorporating IWU simulations into conceptual catchment models can help reduce the uncertainty associated with low-flow simulations, yet it is by no means a substitute for accurate measurement of the actual water withdrawals.~~

6. Conclusion and prospects

Hydrological processes are often poorly defined at the catchment scale due to the limited number of observations at hand and the integral (low-dimensional) nature of these signals (e.g. streamflow). This makes it relatively easy to over-fit the data by adding new hypotheses

1016 to our models, leading to a low degree of falsifiability from a Popperian perspective.
1017 Therefore the incorporation of new processes into a given model structure should be achieved
1018 using as less additional parameters as possible and the same level of mathematical abstraction
1019 as in the original model (as stated in Section 1.4). Ultimately, it is also necessary to show that
1020 this increase in model complexity improves hydrological simulations without increasing
1021 predictive uncertainty.

1022
1023 In the present paper, sublimation losses were incorporated by assuming that the snowpack
1024 can either melt or sublimate. This modeling choice may seem to oversimplify the physics of
1025 snowpacks, yet it allows for the same level of process representation as in commonly-used
1026 empirical melt models. On the whole, this modification helped to reduce errors in the
1027 simulation of snow-cover dynamics at high elevations without increasing the number of
1028 snow-related parameters. However, more research is needed to determine the exact interaction
1029 between snow sublimation and melt in the model. Compared to sublimation losses, the
1030 introduction of irrigation water-use (IWU) increased the overall number of parameters. Yet
1031 this increase in complexity came with additional data (observed phenological dates) to reduce
1032 the number of degrees of freedom. The reliability of probabilistic streamflow predictions was
1033 greatly improved when IWU was explicitly considered, resulting in relatively narrow
1034 uncertainty bands and reduced structural errors. As such, this model modification appears to
1035 be supported by the available data. Incidentally, this approach also provided evidence that
1036 water abstractions from the unregulated Claro River is impacting on the hydrological response
1037 of the system.

1038
1039 One of the main advantages of incorporating IWU is that it provides an estimate of natural
1040 streamflow which can be used to assess the system's capacity to meet increasing irrigation
1041 needs [e.g. Fabre et al., 2015b]. To our knowledge, most of the other approaches used to
1042 'naturalize' influenced streamflow in agricultural catchments do not account for the impacts
1043 of climate variability on crop water-use. Instead, the sum of all historical water rights is
1044 usually taken as an upper bound for the actual water consumption and added back to observed
1045 streamflow before calibrating the model. This makes it difficult to use conceptual catchment
1046 models in climate change impact studies, since changes in temperature patterns are expected
1047 to affect both the timing and volume of irrigation water-use. Depending on their magnitude,
1048 seasonal shifts in the timing of snowmelt runoff and phenological events could result in either
1049 additive or countervailing effects. Earlier peak flows, for instance, could lead to an increase in

1050 water supply at a time when it is not required, or simply compensate for a similar shift in crop
1051 phenology. A new generation of low-dimensional modeling approaches is required to better
1052 understand how these processes interact and evaluate the possibility of selecting the most
1053 suitable varieties and irrigation strategies for a given hydro-climatic context [Duchêne et al.,
1054 2010b; Palliotti et al., 2014]. In this paper, the use of phenological models based on functions
1055 that integrate both the negative and positive effects of higher temperatures on crop
1056 development is suggested as a parsimonious way to improve model robustness in the future.

1057

1058 However, critical challenges remain to be addressed before the model can be used for such
1059 prospective studies. In particular, more research is needed to better separate the effects of
1060 rural land use change from other sources of variability and uncertainty in conceptual
1061 catchment models [McIntyre et al., 2014]. Future work will focus on improving the estimation
1062 of fractional snow-covered areas and the sensitivity of runoff generation components to
1063 intense rainfall and protracted droughts. Results also highlight the need for a better
1064 representation of surface water–groundwater interactions in the routing module. Given the
1065 difficulty in estimating precipitation in the dry Andes, isotope-based studies could
1066 considerably help to quantify the relative contributions of snowmelt, rainfall, ground water
1067 and glacierized areas to streamflow [Ohlanders et al., 2013]. Such understanding is critical to
1068 discriminate between several sources of errors and improve model reliability for use in impact
1069 and adaptation studies.

1070

1071 ~~Increased CO₂ levels are generally expected to improve water-use efficiency at the leaf level~~
1072 ~~by reducing stomatal conductance [Craufurd and Wheeler, 2009]. At the whole plant and~~
1073 ~~catchment scales, however, these positive effects remain highly uncertain due to complex~~
1074 ~~feedbacks occurring within the canopy and in the air above it. The effects of higher~~
1075 ~~temperatures could therefore override those of elevated CO₂ and lead to an overall increase in~~
1076 ~~irrigation water requirements. In mountainous catchments where irrigation water is derived~~
1077 ~~from snowmelt fed rivers, this could generate a growing mismatch between water demand~~
1078 ~~and availability. Depending on their magnitude, seasonal shifts in the timing of peak flows~~
1079 ~~and phenological events could result in either additive or countervailing effects. Earlier peak~~
1080 ~~flows, for instance, could lead to an increase in water supply at a time when it is not required,~~
1081 ~~or simply compensate for a similar shift in crop phenology. A new generation of low-~~
1082 ~~dimensional modeling approaches is required to better understand how these processes~~

1083 ~~interact and evaluate the possibility of selecting the most suitable varieties and irrigation~~
1084 ~~strategies for a given hydro-climatic context [Duchêne et al., 2010b; Palliotti et al., 2014].~~

1085 ~~This study provided a first step toward such efforts in the dry Andes. It also confirmed the~~
1086 ~~difficulty in separating the effects of rural land use change from other sources of variability~~
1087 ~~and uncertainty in conceptual catchment models [McIntyre et al., 2014]. Future work will~~
1088 ~~focus on improving the estimation of fractional snow covered areas and the sensitivity of~~
1089 ~~runoff generation components to intense rainfall and protracted droughts. Results also~~
1090 ~~highlight the need for a better representation of surface water-groundwater interactions in the~~
1091 ~~routing module. Given the difficulty in estimating precipitation in the dry Andes, isotope-~~
1092 ~~based studies could considerably help to quantify the relative contributions of snowmelt,~~
1093 ~~rainfall, ground water and glacierized areas to streamflow [Ohlanders et al., 2013]. Such~~
1094 ~~understanding is critical to discriminate between several sources of errors and improve model~~
1095 ~~reliability for use in impact and adaptation studies.~~

1096

1097 **Appendix A**

1098

1099 Net shortwave and longwave radiations were computed as follows:

$$\Delta R_{SW} = (1 - \alpha)\tau R_e \quad (\text{A.I})$$

$$\Delta R_{LW} = \varepsilon_A \sigma (T_A + 273.15)^4 - \varepsilon_S \sigma (T_S + 273.15)^4 \quad (\text{A.II})$$

1100 where α is the snow albedo, τ is the atmospheric transmissivity, R_e is the extraterrestrial
1101 radiation ($\text{MJ m}^{-2} \text{ day}^{-1}$) calculated from the latitude and the Julian day [Allen et al., 1998], σ
1102 is the Stefan-Boltzmann constant ($4.89 \cdot 10^{-15} \text{ MJ m}^{-2} \text{ K}^{-4}$), ε_S is the longwave emissivity for
1103 snow (0.97) and ε_A is the atmospheric longwave emissivity estimated as in Walter et al.
1104 [2005]. Snow albedo generally decreases between snowfalls as a result of metamorphic
1105 processes. This was represented in the model by adjusting an exponential decay rate related to
1106 the number of days since the last snowfall (N_t):

$$\alpha_t = \alpha_{\min} + (\alpha_{\max} - \alpha_{\min})e^{-k_a N_t} \quad (\text{A.III})$$

1107 where α_{\min} and α_{\max} are the minimum and maximum snow albedos, and k_a is a recession
1108 factor. These parameters were determined from the literature [Lhermitte et al., 2014;
1109 Abermann et al., 2014] to prevent over-fitting (see Table 1). For shallow snowpacks such as
1110 those found around 30°S, albedo values also decrease during snowmelt periods as the
1111 influence of the underlying ground increases. This can have significant effects on melt rates,
1112 which were accounted for implicitly through the V_{\min} parameter in Eq. (5). Based on radiation
1113 data available over the last few years (not shown here), atmospheric transmissivity was set at
1114 0.75 under clear-sky conditions (precipitation < 5 mm) and 0.4 on cloudy days (precipitation
1115 ≥ 5 mm).

1116

1117

1118 **Acknowledgements**

1119 The authors are very grateful to the *Centro de Estudios Avanzados en Zonas Áridas* (CEAZA)
1120 for its essential logistic support during the field missions and to the *Dirección General de*
1121 *Agua* (Chile) for providing the necessary meteorological and streamflow data. P. Hublart was
1122 supported by a national PhD fellowship funded by the French Ministry of Higher Education
1123 and Research. S. Lhermitte was supported as postdoctoral researcher for Fonds
1124 Wetenschappelijk Onderzoek–Vlaanderen. The Matlab program of the Snow Accumulation
1125 and Ablation model is available from the first author on request.

1126 **References**

- 1127 Abermann, J., Kinnard, C., and MacDonell, S.: Albedo variations and the impact of clouds on
1128 glaciers in the Chilean semi-arid Andes, *J. Glaciol.*, 60, 183–191, 2013.
- 1129 Adam, J. C., Hamlet, A. F., and Lettenmaier, D. P.: Implications of global climate change for
1130 snowmelt hydrology in the twenty-first century, *Hydrol. Process.*, 23, 962–972, 2009.
- 1131 Ajami, N. K., Hornberger, G. M., and Sunding, D. L.: Sustainable water resource
1132 management under hydrological uncertainty, *Water Resour. Res.*, 44, W11406,
1133 doi:10.1029/2007WR006736, 2008.
- 1134 Allen, R. G., Smith, M., Perrier, A., and Pereira, L. S.: Crop evapotranspiration – Guidelines
1135 for computing crop water requirements, Irrigation Drainage Paper 56, Food and Agric.
1136 Organ., Rome, Italy, 1998.
- 1137 Andréassian, V., Perrin, C., and Michel, C.: Impact of imperfect potential evapotranspiration
1138 knowledge on the efficiency and parameters of watershed models, *J. Hydrol.*, 286, 19–35,
1139 2004.
- 1140 Ashagrie, A. G., de Laat, P. J., de Wit, M. J., Tu, M. and Uhlenbrook, S.: Detecting the
1141 influence of land use changes on discharges and floods in the Meuse River Basin – the
1142 predictive power of a ninety-year rainfall-runoff relation?, *Hydrol. Earth Syst. Sci.*, 10,
1143 691–701, 2006.
- 1144 Ayala, A., McPhee, J., and Vargas, X.: Altitudinal gradients, midwinter melt, and wind effects
1145 on snow accumulation in semiarid midlatitude Andes under La Niña conditions, *Water*
1146 *Resour. Res.*, 50, 3589–3594, 2014.
- 1147 Ayala, A., Pellicciotti, F., MacDonell, S., McPhee, J., and Burlando, P.: Meteorological
1148 conditions associated to high sublimation amounts in semiarid high-elevation Andes
1149 decrease the performance of empirical melt models, EGU General Assembly 2015, 12–17
1150 April, 2015 in Vienna, Austria, 2015.
- 1151 Beven, K., Smith, P. J., and Wood, A.: On the colour and spin of epistemic error (and what
1152 we might do about it), *Hydrol. Earth Syst. Sci.*, 15, 3123–3133, 2011.
- 1153 Blöschl, G., and Montanari, A.: Climate change impacts – throwing the dice?, *Hydrol.*
1154 *Process.*, 24, 374–381, 2010.
- 1155 Boudhar, A., Hanich, L., Boulet, G., Duchemin, B., Berjamy, B., and Chehbouni, A.:
1156 Evaluation of the Snowmelt Runoff Model in the Moroccan High Atlas Mountains using
1157 two snow-cover estimates, *Hydrol. Sci. J.*, 54, 1094–1113, 2009.

1158 Bourgin, P.-Y ., Andréassian, V., Gascoïn, S., and Valéry, A. : Que sait-on des précipitations
1159 en altitude dans les Andes semi-arides du Chili ?, *Houille Blanche*, 2, 12–17, 2012.

1160 Brigode, P., Oudin, L., and Perrin, C.: Hydrological model parameter instability: A source of
1161 additional uncertainty in estimating the hydrological impacts of climate change?, *J.*
1162 *Hydrol.*, 476, 410–425, 2013.

1163 Brubaker, K., Rango, A., and Kustas, W.: Incorporating radiation inputs into the snowmelt
1164 runoff model, *Hydrol. Process.*, 10, 1329–1343, 1996.

1165 Caffarra, A., and Eccel, E.: Increasing the robustness of phenological models for *Vitis*
1166 *vinifera* cv. Chardonnay, *International Journal of Biometeorology*, 54, 255–267, 2010.

1167 Caffarra, A., and Eccel, E.: Projecting the impacts of climate change on the phenology of
1168 grapevine in a mountain area, *Aust. J. Grape Wine Res.*, 17, 52–61, 2011.

1169 Chuine, I.: A Unified Model for Budburst of Trees, *J. theor. Biol.*, 207, 337–347, 2000.

1170 Cleland, E. E., Chuine, I., Menzel, A., Harold, A. M., and Schwartz, M. D: Shifting plant
1171 phenology in response to global change, *Trends Ecol. Evol.*, 22, 357–365, 2007.

1172 Collet, L., Ruelland, D., Borrell-Estupina, V., Dezetter, A., and Servat, E.: Water supply
1173 sustainability and adaptation strategies under future anthropogenic and climatic changes
1174 of a meso-scale catchment, *Sci. Tot. Env.*, 536, 589–602, 2015.

1175 ~~Craufurd, P. Q., and Wheeler, T. R.: Climate change and the flowering time of annual crops,~~
1176 ~~*J. Exp. Bot.*, 60, 2529–2539, 2009.~~

1177 Duan, Q. Y., Gupta, V. K., and Sorooshian, S.: A shuffled complex evolution approach for
1178 effective and efficient global minimization, *J. Optim. Theory Appl.*, 76, 501–521, 1993.

1179 Duchêne, E., and Schneider, C.: Grapevine and climatic changes: a glance at the situation in
1180 Alsace, *Agron. Sustain. Dev.*, 25, 93–99, 2010a.

1181 Duchêne, E., Huard, F., Dumas, V., Schneider, C., and Merdinoglu, D.: The challenge of
1182 adapting grapevine varieties to climate change, *Clim. Res.*, 41, 193–204, 2010b.

1183 Engeland, K., Renard, B., Steinsland, I., and Kolberg, S.: Evaluation of statistical models for
1184 forecast errors from the HBV model, *J. Hydrol.*, 384, 142–155, 2010.

1185 Fabre, J., Ruelland, D., Dezetter, A., and Grouillet, B.: Accounting for hydro-climatic and
1186 water-use variability in the assessment of past and future water balance at the basin scale,
1187 In: *Hydrologic non-stationarity and extrapolating models to predict the future (Proc. of*
1188 *symp. HS02 held during IUGG2015 in Prague, Czech Republic, June 2015). IAHS Publ.*,
1189 371, 43–48, 2015a.

1190 Fabre, J., Ruelland, D., Dezetter, A., and Grouillet, B.: Simulating past changes in the balance
1191 between water demand and availability and assessing their main drivers at the river basin
1192 scale, *Hydrol. Earth Syst. Sci.*, 19, 1263–1285, 2015b.

1193 Falvey, M., and Garreaud, R. D.: Wintertime precipitation episodes in central Chile:
1194 Associated meteorological conditions and orographic influences, *J. Hydrometeor.*, 8, 171–
1195 193, 2007.

1196 Favier, V., Falvey, M., Rabatel, A., Praderio, E., and López, D.: Interpreting discrepancies
1197 between discharge and precipitation in high-altitude area of Chile's Norte Chico region
1198 (26–32°S), *Water Resour. Res.*, 45, W02424, doi:10.1029/2008WR006802, 2009.

1199 Fenicia, F., Kavetski, D., and Savenije, H. H. G.: Elements of a flexible approach for
1200 conceptual hydrological modeling: 1. Motivation and theoretical development, *Water
1201 Resour. Res.*, 47, W11510, doi:10.1029/2010WR010174, 2011.

1202 Fila, G., Di Lena, B., Gardiman, M., Storchi, P., Tomasi, D., Silvestroni, O., and Pitacco, A.:
1203 Calibration and validation of grapevine budburst models using growth-room experiments
1204 as data source, *Agr. Forest. Meteorol.*, 160, 69–79, 2012.

1205 Fila, G., Gardiman, M., Belvini, P., Meggio, F., and Pitacco, A.: A comparison of different
1206 modelling solutions for studying grapevine phenology under present and future climate
1207 scenarios, *Agr. Forest. Meteorol.*, 195–196, 192–205, 2014.

1208 Fontaine, T. A., Cruickshank, T. S., Arnold, J. G., and Hotchkiss, R. H.: Development of a
1209 snowfall-snowmelt routine for mountainous terrain for the soil water assessment tool
1210 (SWAT), *J. Hydrol.*, 262, 209–223, 2002.

1211 García de Cortázar-Atauri, I., Daux, V., Garnier, E., Yiou, P., Viovy, N., Seguin, B.,
1212 Boursiquot, J. M., Parker, A. K., van Leeuwen, C., and Chuine, I.: Climate reconstructions
1213 from grape harvest dates: Methodology and uncertainties, *The Holocene* 20, 599–608,
1214 2010.

1215 Gascoin, S., Lhermitte, S., Kinnard, C., Bortels, K., and Liston, G. E.: Wind effects on snow
1216 cover in Pascua-Lama, Dry Andes of Chile, *Adv. Water Resour.*, 55, 25–39, 2013.

1217 Gelman, A. G., and Rubin, D. B.: Inference from iterative simulation using multiple
1218 sequences, *Stat. Sci.* 7, 457–472, 1992.

1219 Gharari, S., Hrachowitz, M., Fenicia, F., Gao, H., and Savenije, H. H. G.: Using expert
1220 knowledge to increase realism in environmental system models can dramatically reduce
1221 the need for calibration, *Hydrol. Earth Syst. Sci.*, 18, 4839 – 4859, 2014.

1222 Greer, D. H., and Weedon, M. M.: The impact of high temperatures on *Vitis vinifera* cv.
1223 Semillon grapevine performance and berry ripening, *Front. Plant Sci.*, 4, 491, 2013.

- 1224 Gupta, H. V., Kling, H., Yilmaz, K. K., and Martinez, G. F.: Decomposition of the mean
1225 squared error and NSE performance criteria: Implications for improving hydrological
1226 modelling, *J. Hydrol.*, 377, 80–91, 2009.
- 1227 Harshburger, B. J., Humes, K. S., Walden, V. P., Moore, B. C., Blandford, T. R., and Rango,
1228 A.: Evaluation of Short-to-Medium Range Streamflow Forecasts Obtained Using an
1229 Enhanced Version of SRM, *J. Am. Water Resour. Assoc.*, 46, 603–617, 2010.
- 1230 Hendrickson, L., Ball, M. C., Wood, J. T., Chow, W. S., and Furbank, R. T.: Low temperature
1231 effects on photosynthesis and growth of grapevine, *Plant Cell Environ.*, 27, 795–809,
1232 2004.
- 1233 Hock, R.: Temperature index melt modelling in mountain areas, *J. Hydrol.*, 282, 104–115,
1234 2003.
- 1235 Hublart, P., Ruelland, D., Dezetter, A., and Jourde, H.: Reducing structural uncertainty in
1236 conceptual hydrological modeling in the semi-arid Andes, *Hydrol. Earth Syst. Sci.*, 19,
1237 2295–2314, 2015a.
- 1238 [Hublart, P., Ruelland, D., García De Cortázar Atauri, I., and Ibacache, A.: Reliability of a
1239 conceptual hydrological model in a semi-arid Andean catchment facing water-use
1240 changes, *Proc. IAHS*, 371, 203–209, 2015b.](#)
- 1241 Hughes, D. A., and Mantel, S. K.: Estimating the uncertainty in simulating the impacts of
1242 small farm dams on streamflow regimes in South Africa, *Hydrol. Sci. J.*, 55, 578–592,
1243 2010.
- 1244 Ibacache, A.: Cómo influye la temperatura sobre la época de cosecha en vides, *Tierra
1245 Adentro*, 81, 8–10, 2008.
- 1246 Ibacache, A., Martínez, L., Sturla, C., and Montes, C.: Zonificación del territorio de la
1247 denominación de origen Pisco, *Nuestro Pisco*, Programa de Innovación Territorial,
1248 Informe Final, 2010.
- 1249 Jin, X., Xu, C.-Y., Zhang, Q., and Singh, V. P.: Parameter and modeling uncertainty
1250 simulated by GLUE and a formal Bayesian method for a conceptual hydrological model,
1251 *J. Hydrol.*, 383, 147–155, 2010.
- 1252 Jones, G. V., White, M. A., Cooper, O. R., and Storchmann, K.: Climate change and global
1253 wine quality, *Climatic Change*, 73, 319–343, 2005.
- 1254 Kalthoff, N., Fiebig-Wittmaack, M., Meißner, C., Kohler, M., Uriarte, M., Bischoff-Gauß, I.,
1255 and Gonzales, E.: The energy balance, evapo-transpiration and nocturnal dew deposition
1256 of an arid valley in the Andes, *J. Arid Environ.*, 65, 420–443, 2006.

- 1257 Kim, H. S., Croke, B. F. W., Jakeman, A. J., Chiew, F., and Mueller, N.: Towards separation
1258 of climate and land use effects on hydrology: data analysis of the Googong and Cotter
1259 Catchments, In: Oxley, L., Kulasiri, D. (Eds.), MODSIM 2007 International Congress on
1260 Modelling and Simulation, Modelling and Simulation Society of Australia and New
1261 Zealand, 74–80, 2007.
- 1262 Kiptala, J. K., Mul, M. L., Mohamed, Y. A., and van der Zaag, P.: Modelling stream flow and
1263 quantifying blue water using a modified STREAM model for a heterogeneous, highly
1264 utilized and data-scarce river basin in Africa, *Hydrol. Earth Syst. Sci.* 18, 2287–2303,
1265 2014.
- 1266 Koskela, J. J., Croke, B. W. F., Koivusalo, H., Jakeman, A. J., and Kokkonen, T.: Bayesian
1267 inference of uncertainties in precipitation-streamflow modeling in a snow affected
1268 catchment, *Water Resour. Res.*,48, W11513, doi:10.1029/2011WR011773, 2012.
- 1269 Laio, F., and Tamea, S.: Verification tools for probabilistic forecasts of continuous
1270 hydrological variables, *Hydrol. Earth Syst. Sci.*, 11, 1267–1277, 2007.
- 1271 Le Moine, N., Andréassian, V., Perrin, C., and Michel, C.: How can rainfall-runoff models
1272 handle intercatchment groundwater flows? Theoretical study based on 1040 French
1273 catchments, *Water Resour. Res.* 43, W06428, doi:10.1029/2006WR005608, 2007.
- 1274 Lhermitte, S., Abermann, J., and Kinnard, C.: Albedo over rough snow and ice surfaces,
1275 *Cryosphere* 8, 1069–1086, 2014.
- 1276 L'hôte, Y., Chevallier, P., Coudrain, A., Lejeune, Y., and Etchevers, P.: Relationship between
1277 precipitation phase and air temperature: comparison between the Bolivian Andes and the
1278 Swiss Alps, *Hydrol. Sci. J.*, 50, 989–997, 2005.
- 1279 MacDonell, S., Kinnard, C., Mölg, T., Nicholson, L., and Abermann, J.: Meteorological
1280 drivers of ablation processes on a cold glacier in the semiarid Andes of Chile, *The*
1281 *Cryosphere*, 7, 1833–1870, 2013.
- 1282 McIntyre, N., Ballard, C., Bruen, M., Bulygina, N., Buytaert, W., Cluckie, I., Dunn, S., Ehret,
1283 U., Ewen, J., Gelfan, A., Hess, T., Hughes, D., Jackson, B., Kjeldsen, T. R., Merz, R.,
1284 Park, J.-S., O'Connell, E., O'Donnell, G., Oudin, L., Todini, E., Wagener, T., and
1285 Wheeler, H.: Modelling the hydrological impacts of rural land use change, *Hydrol. Res.*,
1286 45, 737–754, 2014.
- 1287 Merritt, W. S., Croke, B. F. W., Jakeman, A. J., Letcher, R. A., and Perez, P.: A biophysical
1288 toolbox for assessment and management of land and water resources in rural catchments
1289 in northern Thailand, *Ecol. Model.*, 171, 279–300, 2004.

1290 Montanari, A.: Interactive comment on “ On the colour and spin of epistemic error (and what
1291 we might do about it)”, *Hydrol. Earth Syst. Sci.* 15, 3123–3133, 2011.

1292 Montecinos, A., and Aceituno, P.: Seasonality of the ENSO-Related Rainfall Variability in
1293 Central Chile and Associated Circulation Anomalies, *J. Climate*, 16, 281–296, 2003.

1294 Nicolle, P., Pushpalatha, R., Perrin, C., Francois, D., Thiéry, D., Mathevet, T., Le Lay, M.,
1295 Besson, F., Soubeyroux, J. M., Viel, C., Regimbeau, F., Andréassian, V., Maugis, P.,
1296 Augeard, B., and Morice, E.: Benchmarking hydrological models for low-flow simulation
1297 and forecasting on French catchments, *Hydrol. Earth Syst. Sci.*, 18, 2829–2857, 2014.

1298 Ohlanders, N., Rodriguez, M., and McPhee, J.: Stable water isotope variation in a Central
1299 Andean watershed dominated by glacier and snowmelt, *Hydrol. Earth Syst. Sci.*, 17,
1300 1035–1050, 2013.

1301 Ohmura, A.: Physical Basis for the Temperature-Based Melt-Index Method, *J. Appl.*
1302 *Meteor.*, 40, 753–761, 2001.

1303 Oudin, L., Hervieu, F., Michel, C., Perrin, C., Andreassian, V., Anctil, F., and Loumagne, C.:
1304 Which potential evapotranspiration input for a lumped rainfall-runoff model? Part 2:
1305 towards a simple and efficient potential evapotranspiration model for rainfall-runoff
1306 modelling, *J. Hydrol.*, 303, 290–306, 2005.

1307 Oudin, L., Perrin, C., Mathevet, T., Andréassian, V., and Michel, C.: Impact of biased and
1308 randomly corrupted inputs on the efficiency and the parameters of watershed models, *J.*
1309 *Hydrol.*, 320, 62–83, 2006.

1310 Palliotti, A., Tombesi, S., Silvestroni, O., Lanari, V., Gatti, M., and Poni, S.: Changes in
1311 vineyard establishment and canopy management urged by earlier climate-related grape
1312 ripening: A review, *Sci. Hort.*, 178, 43–54, 2014.

1313 Parker, A., Garcia de Cortázar-Atauri, I., Chuine, I., Barbeau, G., Bois, B., Boursiquot, J. M.,
1314 Cahurel, J. Y., Claverie, M., Dufourcq, T., Gény, L., Guimberteau, G., Hofmann, R. W.,
1315 Jacquet, O., Lacombe, T., Monamy, C., Ojeda, H., Panigai, L., Payan, J. C., Lovelle, B.
1316 R., Rouchaud, E., Schneider, C., Spring, J. L., Storchi, P., Tomasi, D., Trambouze, W.,
1317 Trought, M., and van Leeuwen, C.: Classification of varieties for their timing of flowering
1318 and veraison using a modelling approach: A case study for the grapevine species *Vitis*
1319 *vinifera* L., *Agric. For. Meteorol.*, 180, 249–264, 2013.

1320 Pellicciotti, F., Helbing, J., Rivera, A., Favier, V., Corripio, J., Araos, J., Sicart, J. E., and
1321 Careno, M.: A study of the energy balance and melt regime on Juncal Norte Glacier,
1322 semi-arid Andes of central Chile, using melt models of different complexity, *Hydrol.*
1323 *Process.*, 22, 3980–3997, 2008.

1324 Perrin, C., Michel, C. and Andréassian, V.: Improvement of a parsimonious model for
1325 streamflow simulation, *J. Hydrol.*, 279, 275–289, 2003.

1326 Pushpalatha, R., Perrin, C., Le Moine, N., and Andréassian, V.: A downward structural
1327 sensitivity analysis of hydrological models to improve low-flow simulation, *J. Hydrol.*,
1328 411, 66–76, 2011.

1329 Pushpalatha, R., Perrin, C., Le Moine, N., Mathevet, T., and Andréassian, V.: A review of
1330 efficiency criteria suitable for evaluating low-flow simulations, *J. Hydrol.*, 420–421, 171–
1331 182, 2012.

1332 Ruelland, D., Dezetter, A., and Hublart, P.: Sensitivity analysis of hydrological modelling to
1333 climate forcing in a semi-arid mountainous catchment, In: *Hydrology in a changing world:
1334 environmental and human dimensions (Proc. 7th FRIEND-Water Int. Conf., Montpellier,
1335 France, 7–10 Oct. 2014)*, IAHS Publ., 363, 145–150, 2014.

1336 Salinas, C. X., Gironás, J., and Pinto, M.: Water security as a challenge for the sustainability
1337 of La Serena-Coquimbo conurbation in northern Chile: global perspectives and
1338 adaptation, *Mitig. Adapt. Strateg. Glob. Change*, DOI 10.1007/s11027-015-9650-3, 2015.

1339 Savenije, H. H. G.: HESS Opinions "Topography driven conceptual modelling (FLEX-
1340 Topo)", *Hydrol. Earth Syst. Sci.*, 14, 2681–2692, 2010.

1341 Scanlon, B. R., Keese, K. E., Flint, A. L., Flint, L. E., Gaye, C. B., Edmunds, M. W., and
1342 Simmers, I.: Global synthesis of groundwater recharge in semiarid and arid regions,
1343 *Hydrol. Process.*, 20, 3335–3370, 2006.

1344 Schaefli, B., and Huss, M.: Integrating point glacier mass balance observations into
1345 hydrologic model identification, *Hydrol. Earth Syst. Sci.*, 15, 1227–1241, 2011.

1346 Schoups, G., and Vrugt, J. A.: A formal likelihood function for parameter and predictive
1347 inference of hydrologic models with correlated, heteroscedastic, and non-Gaussian
1348 errors, *Water Resour. Res.*, 46, W10531, doi:10.1029/2009WR008933, 2010.

1349 Schulz, N., Boisier, J. P., and Aceituno, P.: Climate change along the arid coast of northern
1350 Chile, *Int. J. Climatol.*, 32, 1803–1814, 2011.

1351 Schulz, O., and de Jong, C.: Snowmelt and sublimation: field experiments and modelling in
1352 the High Atlas Mountains of Morocco, *Hydrol. Earth Syst. Sci.*, 8, 1076–1089, 2004.

1353 Seibert, J., and McDonnell, J. J.: Land-cover impacts on streamflow: a change-detection
1354 modelling approach that incorporates parameter uncertainty, *Hydrol. Sci. J.*, 55, 316–332,
1355 2010.

1356 Siebert, S., and Döll, P.: Quantifying blue and green virtual water contents in global crop
1357 production as well as potential production losses without irrigation, *J. Hydrol.*, 384, 198–
1358 217, 2010.

1359 Smith, T., Sharma, A., Marshall, L., Mehrotra, R., and Sisson, S.: Development of a formal
1360 likelihood function for improved Bayesian inference of ephemeral catchments, *Water*
1361 *Resour. Res.* 46, W12551, doi:10.1029/2010WR009514, 2010.

1362 Sproles, E., Nolin, A. W., Rittger, K., and Painter, T. H.: Climate change impacts on maritime
1363 mountain snowpack in the Oregon Cascades, *Hydrol. Earth Syst. Sci.*, 17, 2581–2597,
1364 2013.

1365 Squeo, F. A., Veit, H., Arancio, G., Gutiérrez, J. R., Arroyo, M. T. K., and Olivares, N.:
1366 Spatial heterogeneity of high mountain vegetation in the Andean desert zone of Chile (30°
1367 S), *Mt. Res. Dev.*, 13, 203–209, 1993.

1368 Staudinger, M., Stahl, K., Seibert, J., Clark, M. P., and Tallaksen, L. M.: Comparison of
1369 hydrological model structures based on recession and low flow simulations, *Hydrol. Earth*
1370 *Syst. Sci.*, 15, 3447–3459, 2011.

1371 Stehr, A., Debels, P., Arumi, J. L., Romero, F., and Alcayaga, H.: Combining the Soil and
1372 Water Assessment Tool (SWAT) and MODIS imagery to estimate monthly flows in a
1373 datascarc Chilean Andean basin, *Hydrol. Sci. J.*, 54, 1053–1067, 2009.

1374 Thyer, M., Renard, B., Kavetski, D., Kuczera, G., Franks, S. W., and Srikanthan, S.: Critical
1375 evaluation of parameter consistency and predictive uncertainty in hydrological modeling:
1376 A case study using Bayesian total error analysis, *Water Resour. Res.*, 45, W00B14,
1377 doi:10.1029/2008WR006825, 2009.

1378 Valéry, A., Andréassian, V., and Perrin, C.: Regionalization of precipitation and air
1379 temperature over high-altitude catchments – learning from outliers, *Hydrol. Sci. J.*, 55,
1380 928–940, 2010a.

1381 Valéry, A.: Modélisation précipitations – débit sous influence nivale Elaboration d’un module
1382 neige et évaluation sur 380 bassins versants, PhD Thesis, Irstea, Paris: AgroParisTech,
1383 2010b.

1384 Valéry, A., Andréassian, V., and Perrin, C.: As simple as possible but not simpler: What is
1385 useful in a temperature-based snow-accounting routine? Part 2 – Sensitivity analysis of
1386 the Cemaneige snow accounting routine on 380 catchments, *J. Hydrol.*, 517, 1176–1187,
1387 2014.

- 1388 Verbist, K., Robertson, A. W., Cornelis, W. M., and Gabriels, D.: Seasonal predictability of
1389 daily rainfall characteristics in central northern Chile for dry-land management, *J. Appl.*
1390 *Meteorol. Clim.*, 49, 1938–1955, 2010.
- 1391 Villagra, P., García de Cortázar, V., Ferreyra, R., Aspillaga, C., Zúñiga, C., Ortega-Farias, S.,
1392 and Sellés, G.: Estimation of water requirements and Kc values of ‘Thompson Seedless’
1393 table grapes grown in the overhead trellis system, using the Eddy covariance method,
1394 *Chil. J. Agr. Res.*, 74, 213–218, 2014.
- 1395 Vrugt, J. A., ter Braak, C. J. F., Diks, C. G. H., Higdon, D., Robinson, B. A., and Hyman, J.
1396 M.: Accelerating Markov chain Monte Carlo simulation by differential evolution with
1397 self-adaptive randomized subspace sampling, *Int. J. Nonlin. Sci. Num.*, 10, 271–288,
1398 2009.
- 1399 Walter, M. T., Brooks, E. S., McCool, D. K., King, L. G., Molnau, M., and Boll, J.: Process-
1400 based snowmelt modeling : does it require more input data than temperature-index
1401 modeling?, *J. Hydrol.*, 300, 65–75, 2005.
- 1402 Wagener, T., Boyle, D. P., Lees, M. J., Wheeler, H. S., Gupta, H. V., and Sorooshian, S.: A
1403 framework for development and application of hydrological models, *Hydrol. Earth*
1404 *System Sci.*, 5, 13–26, 2001.
- 1405 Wang, E., and Engel, T.: Simulation of Phenological Development of Wheat Crops, *Agric.*
1406 *Syst.*, 58, 1–24, 1998.
- 1407 Wang, Q. J., Robertson, D. E., and Chiew, F. H. S.: A Bayesian joint probability modeling
1408 approach for seasonal forecasting of streamflows at multiple sites, *Water Resour. Res.*, 45,
1409 W05407, doi:10.1029/2008WR007355, 2009.
- 1410 Webb, L. B., Whetton, P. H., and Barlow, E. W. R.: Modelled impact of future climate
1411 change on the phenology of winegrapes in Australia, *Aust. J. Grape Wine Res.*, 13, 165–
1412 175, 2007.
- 1413 Yang, T., Xu, C. Y., Shao, Q. X., Chen, X., Lu, G. H., and Hao, Z. C.: Temporal and spatial
1414 patterns of low-flow changes in the Yellow River in the last half century, *Stoch. Environ.*
1415 *Res. Risk Assess.*, 24, 297–309, 2010.

1416

1417 **TABLES & CAPTIONS**

1418

1419 **Table 1** Initial range or value of each model parameter. The second-third column provides explanations on the
 1420 meaning of the parameters and their units (in brackets). The third-fourth column indicates whether parameters
 1421 are calibrated or fixed beforehand. (*) For more details on the GL function, see Schoups and Vrugt [2010].
 1422

Parameter	Model	Signification Meaning	Calibration	Initial range or value
Phenological models (calibrated against observed phenological dates)				
t_0	UniChill	Starting date for chilling rates accumulation (-)	No	15 th April
a	UniChill	Shape parameter of the chilling bell-curve (-)	Yes	0.1 – 2
b	UniChill	Optimal chilling temperature (°C)	Yes	0 – 20
c	UniChill	Shape parameter of the sigmoidal curve (-)	No	-0.25
d	UniChill	Shape parameter of the sigmoidal curve (°C)	No	15
C_{BB}	UniChill	Critical chilling requirement (-)	Yes	4 – 100
F_{BB}	UniChill	Critical state of forcing for budburst (-)	Yes	10 – 200
T_{min}	WE	Minimum temperature (°C)	No	0
T_{opt}	WE	Optimum temperature (°C)	Yes	0 – 40
T_{max}	WE	Maximum temperature (°C)	No	40
F_{FB}	WE	Critical state of forcing for full bloom (-)	Yes	1 – 300
F_{HV}	WE	Critical state of forcing for harvest (-)	Yes	1 – 300
Hydrological models (calibrated against observed streamflow data)				
θ_s	SAA	Snowpack cold-content factor (-)	Yes	0 – 1
MF	SAA	Restricted melt factor (mm day ⁻¹)	Yes	0 – 20
T_{thr}	SAA	Snowmelt temperature threshold (°C)	No	0
α_{min}	SAA	Minimum snow albedo (-)	No	0.4
α_{max}	SAA	Maximum snow albedo (-)	No	0.8
k_a	SAA	Time-scale parameter for the albedo (day ⁻¹)	No	0.25
$X1$	GR4J	Capacity of the soil-moisture accounting store (mm)	Yes	0 – 2000
$X2$	GR4J	Groundwater exchange coefficient (mm)	Yes	-10 – 10
$X3$	GR4J	Capacity of the routing store (mm)	Yes	0 – 500
$X4$	GR4J	Unit hydrograph time base (day)	Yes	0 – 10
$K_{C,BB}$	IWU	Crop coefficient at budburst (-)	No	0
$K_{C,FB}$	IWU	Crop coefficient at full bloom (-)	No	0.7
$K_{C,HV}$	IWU	Crop coefficient at harvest (-)	No	1.4
$K_{C,LF}$	IWU	Crop coefficient at the end of leaf fall (-)	No	0
N_{LF}	IWU	Length of the post-harvest period (day)	No	60 (Moscatel Rosada) 120 (Flame Seedless)
Generalized Likelihood function (inferred together with the hydrological parameters) (*)				
σ_0	GL	Heteroscedasticity intercept (mm day ⁻¹)	Yes	0 – 1
σ_1	GL	Heteroscedasticity slope (-)	Yes	0 – 1
Φ_1	GL	Autocorrelation coefficient (-)	Yes	0 – 0.8
β	GL	Kurtosis parameter (-)	Yes	-1 – 1
ε	GL	Skewness parameter (-)	No	1
μ_b	GL	Bias parameter (mm day ⁻¹)	No	0

1423

1424 **Table 2** Goodness-of-fit (calibration) and predicting performance (validation) of the phenological models.
 1425 RMSE, Root Mean Square Error; NSE, Nash-Sutcliffe Efficiency; Bias, mean difference between the observed
 1426 and predicted dates.

1427

Model	Calibration (whole dataset)						Leave-one-out cross-validation					
	Flame Seedless			Moscatel Rosada			Flame Seedless			Moscatel Rosada		
	RMSE (days)	NSE (-)	Bias (days)	RSME (days)	NSE (-)	Bias (days)	RMSE (days)	NSE (-)	Bias (days)	RMSE (days)	NSE (-)	Bias (days)
BB	3.0	0.89	0.3	3.4	0.80	-0.29	5.4	0.64	0.4	6.8	0.18	0.6
FB	6.0	0.16	-0.6	6.1	0.46	0.5	7.0	-0.13	-0.1	7.2	0.24	0.13
HV	4.0	0.51	0.5	3.4	0.92	0.0	5.2	0.16	0.7	7.9	0.55	2.2

1428

1429 **Table 3** Calibrated parameter values of the phenological models

1430

Variety	Budburst				Full bloom		Harvest	
	a (°C ⁻¹)	b (°C)	C_{BB} (-)	F_{BB} (-)	T_{opt} (°C)	F_{FB} (-)	T_{opt} (°C)	F_{HV} (-)
Flame Seedless	0.11	11.5	27.4	21.2	22.0	55.5	30.2	28.9
Moscatel Rosada	0.57	11.3	10.8	41.8	20.2	49.9	32.9	31.3

1431

1432 **Table 4** Goodness-of-fit (calibration) and predicting performance (validation) of the hydrological models.

1433

Model	Calibration (1985–1995)				Validation (1985–1995)				Snow Errors (%) (2000–2011)				
	F _{obj} (-)	KGE _{inv} (-)	NSE (-)	RMSE (m ³ s ⁻¹)	F _{obj} (-)	KGE _{inv} (-)	NSE (-)	RMSE (m ³ s ⁻¹)	EZ 1 (%)	EZ 2 (%)	EZ 3 (%)	EZ 4 (%)	EZ 5 (%)
A	0.13	0.77	0.94	1.66	0.27	0.53	0.88	2.66	2	15	16	12	17
B	0.16	0.74	0.93	1.76	0.33	0.43	0.90	2.41	2	16	16	10	11
C	0.07	0.90	0.95	1.55	0.13	0.80	0.90	2.36	2	16	16	10	11

1434

1435 **Table 5** Sublimation rates and contribution to snow ablation over the period 2000–2011.

1436

Model	Mean annual sublimation rates (mm day ⁻¹)					Sublimation / Ablation ratio (%)				
	EZ 1	EZ 2	EZ 3	EZ 4	EZ 5	EZ 1	EZ 2	EZ 3	EZ 4	EZ 5
B	0.00	0.07	0.30	0.75	1.11	0	4	11	26	36
C	0.00	0.07	0.31	0.75	1.11	0	4	12	26	37

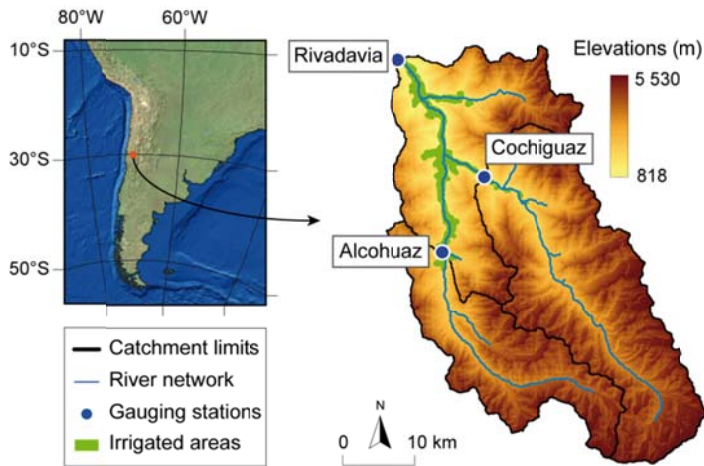
1437

1438 **FIGURES & CAPTIONS**

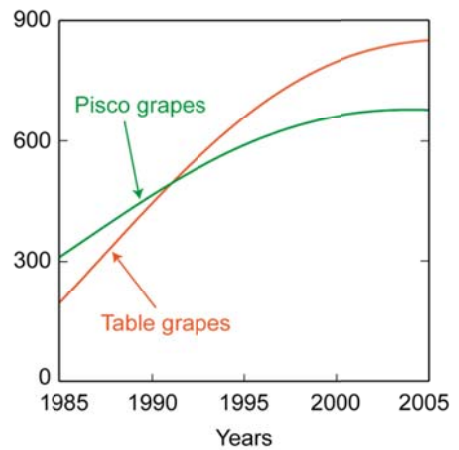
1439

1440 **Figure 1** The Claro River catchment, Chile (30°S): (a) topography and current location of irrigated areas, (b)
 1441 evolution of irrigated areas since 1985 (interpolated from local cadastral surveys) for both types of grapes, and
 1442 (c) potential effects of increased irrigation water-use on mean annual hydrographs since the mid-1990s. These
 1443 effects were estimated from the difference between streamflow measured at the outlet in Rivadavia (in black)
 1444 and that measured at Cochiguaz and Alcohuaz (in red), which remains largely unaltered.
 1445

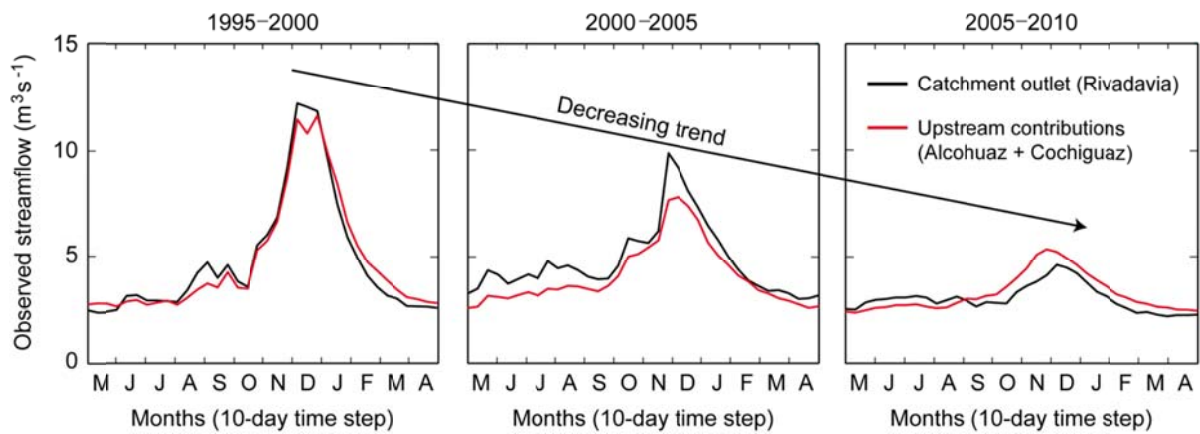
(a) Catchment map and location of irrigated areas



(b) Evolution of irrigated areas (ha)



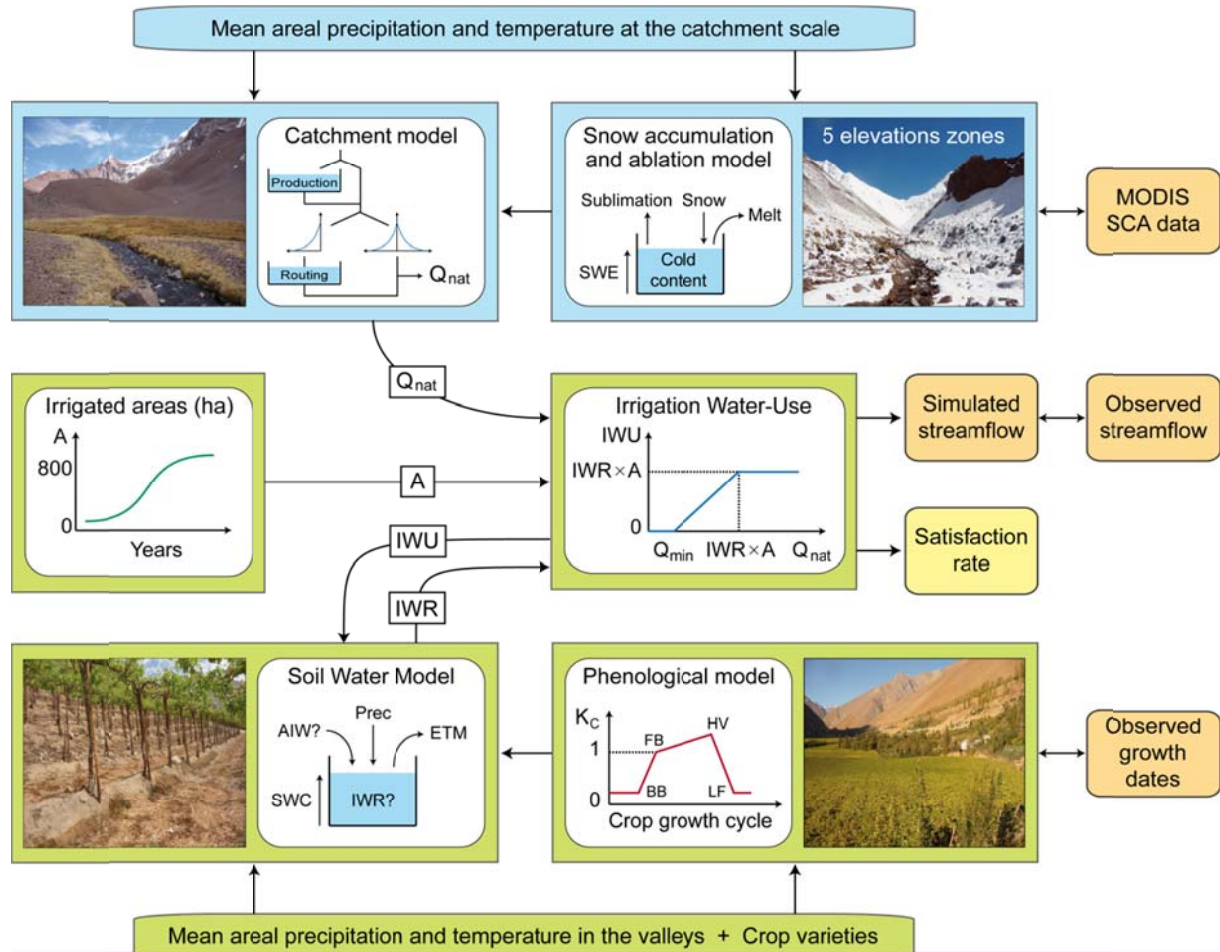
(c) Potential impacts of irrigation water-use on the catchment response



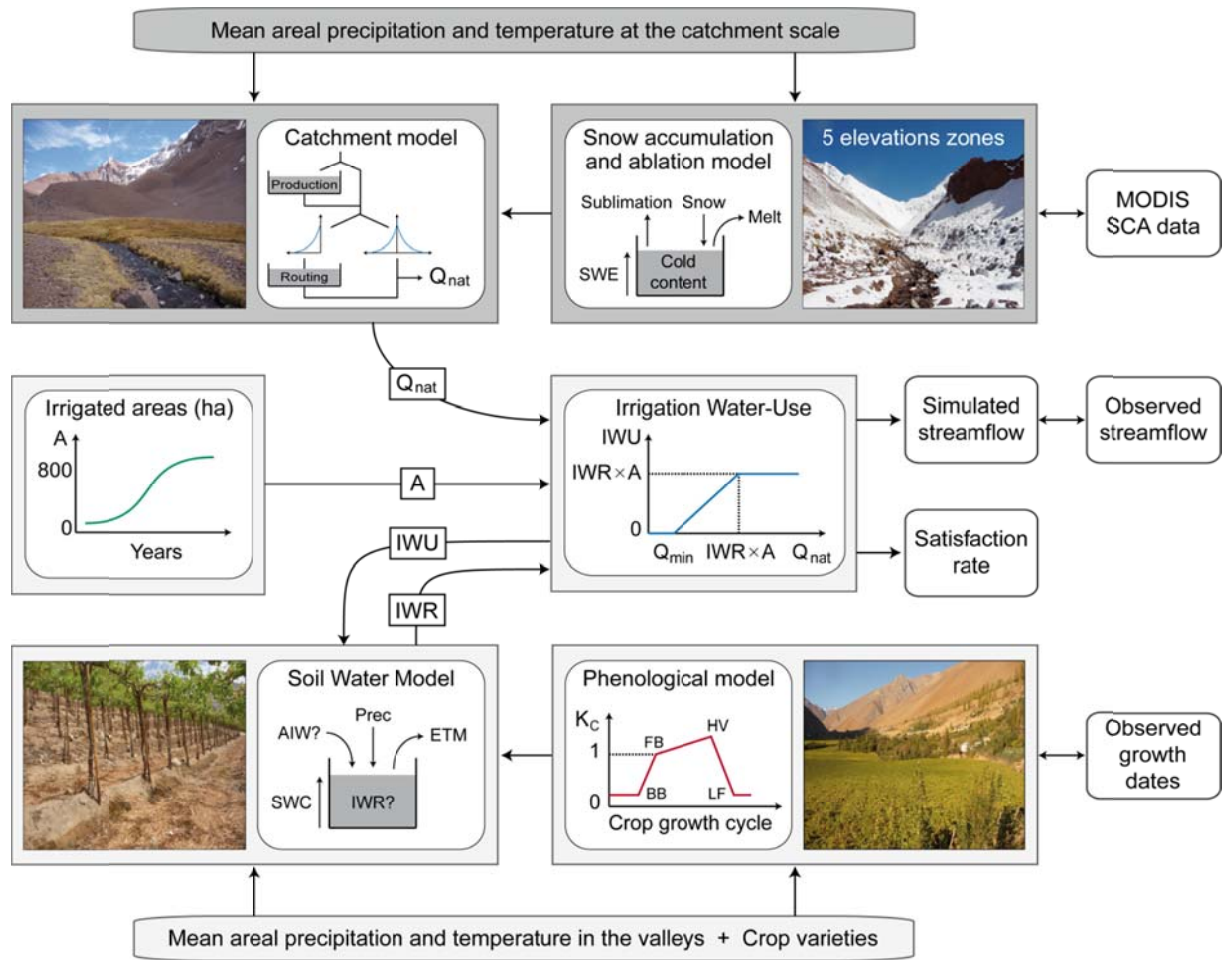
1446

1447

1448 **Figure 2** Block diagram of the lumped modeling framework developed in this study. The blue blocks refer to the hydrological part of the framework (used by Models A, B and C) while the green blocks relate to the estimation
 1449 of irrigation water requirements and irrigation water-use (used only by Model C). The simulated outputs and
 1450 observed data used for calibration/validation are indicated in orange. A satisfaction rate can also be computed
 1451 based on the ratio between water availability and irrigation requirements.
 1452
 1453

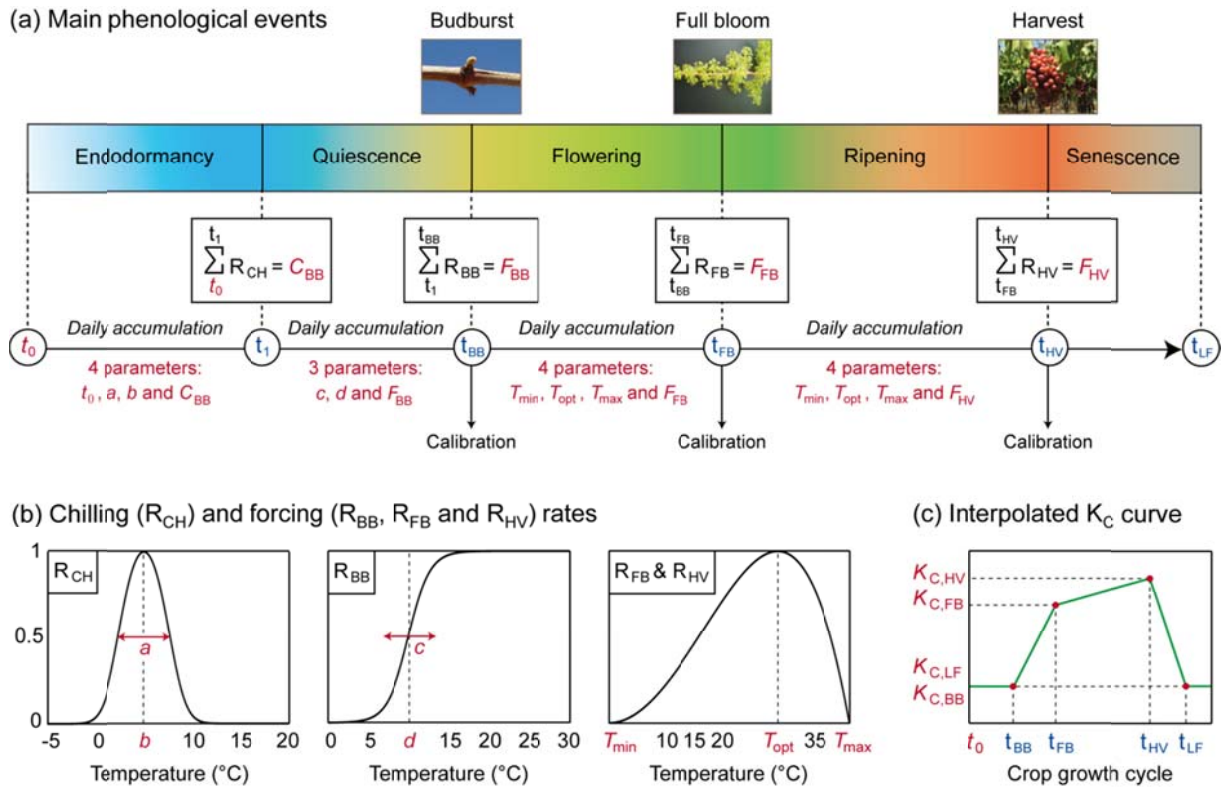


1454
 1455
 1456



1457

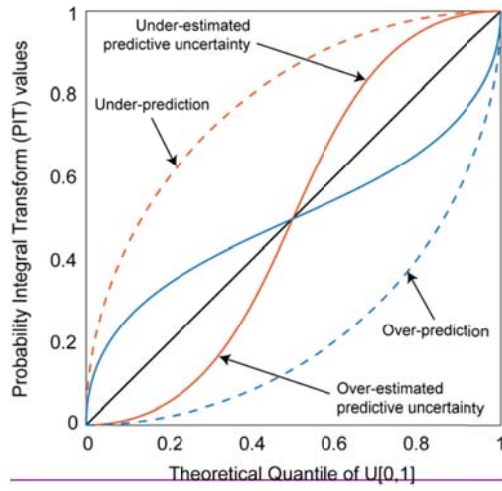
1458 **Figure 3** Crop growth and water requirements modeling framework: (a) partitioning of the growing season into five phenophases and parameterization of each phenophase, (b) functions used to express the accumulated
 1459 chilling and forcing rates over each phenophase, and (c) translation of the simulated dates of budburst, full
 1460 bloom and harvest into an interpolated K_C curve for use in the IWU model. Model parameters are indicated in
 1461 italic and colored in red. Note that parameters t_0 , c , d , T_{min} , T_{max} , $K_{C,BB}$, $K_{C,FB}$, $K_{C,HV}$ and $K_{C,LF}$ were fixed
 1462 beforehand to avoid over-parameterization.
 1463
 1464



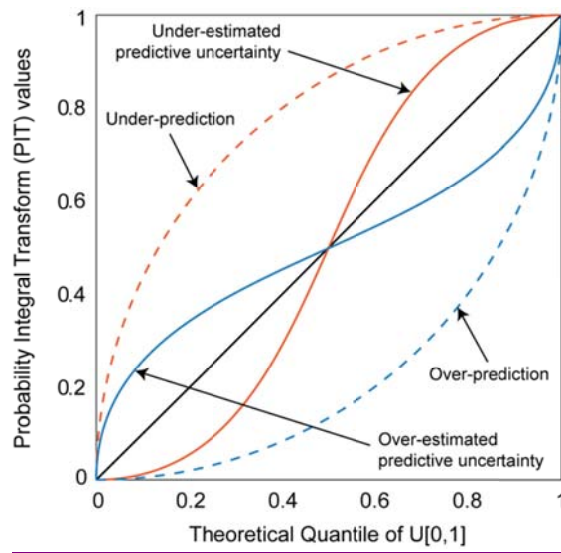
1465

1466

1467 | **Figure 4** Possible interpretations of PIT plots (modified from Laio and Tamea [2007]). The diagonal line (in
1468 | black) represents the ideal case.
1469 |

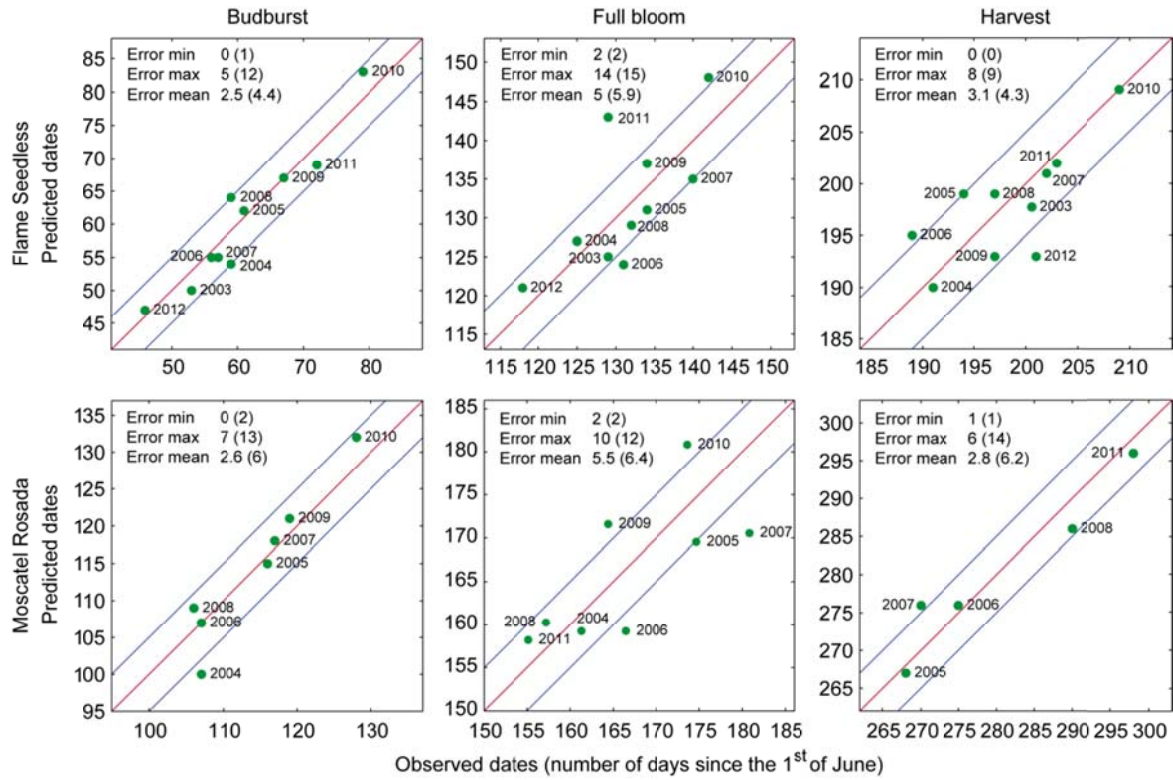


1470 |
1471 |



1472 |

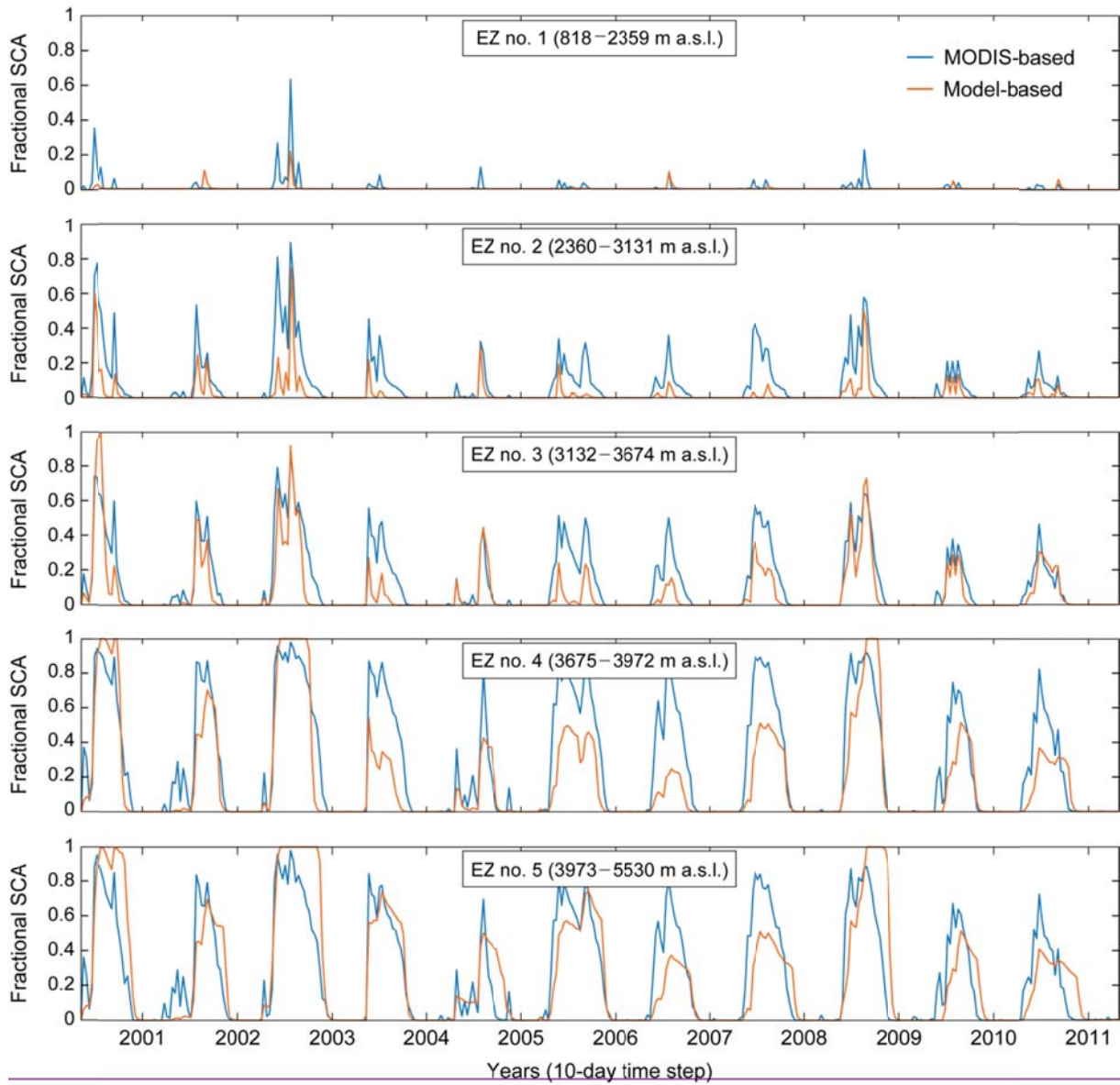
1473 **Figure 5** Observed vs. predicted dates of budburst, full bloom and harvest for Flame Seedless and Moscatel
 1474 Rosada at the INIA experimental site. The dates are expressed in number of days since the 1st of June. The
 1475 minimum, maximum and mean absolute errors (in days) are given for each variety and stage of growth (the
 1476 values between brackets relate to the validation step while the values in front of the brackets relate to the
 1477 calibration step). The upper and lower blue lines indicate delays of ± 5 days between observed and predicted
 1478 dates, respectively.
 1479



1480

1481

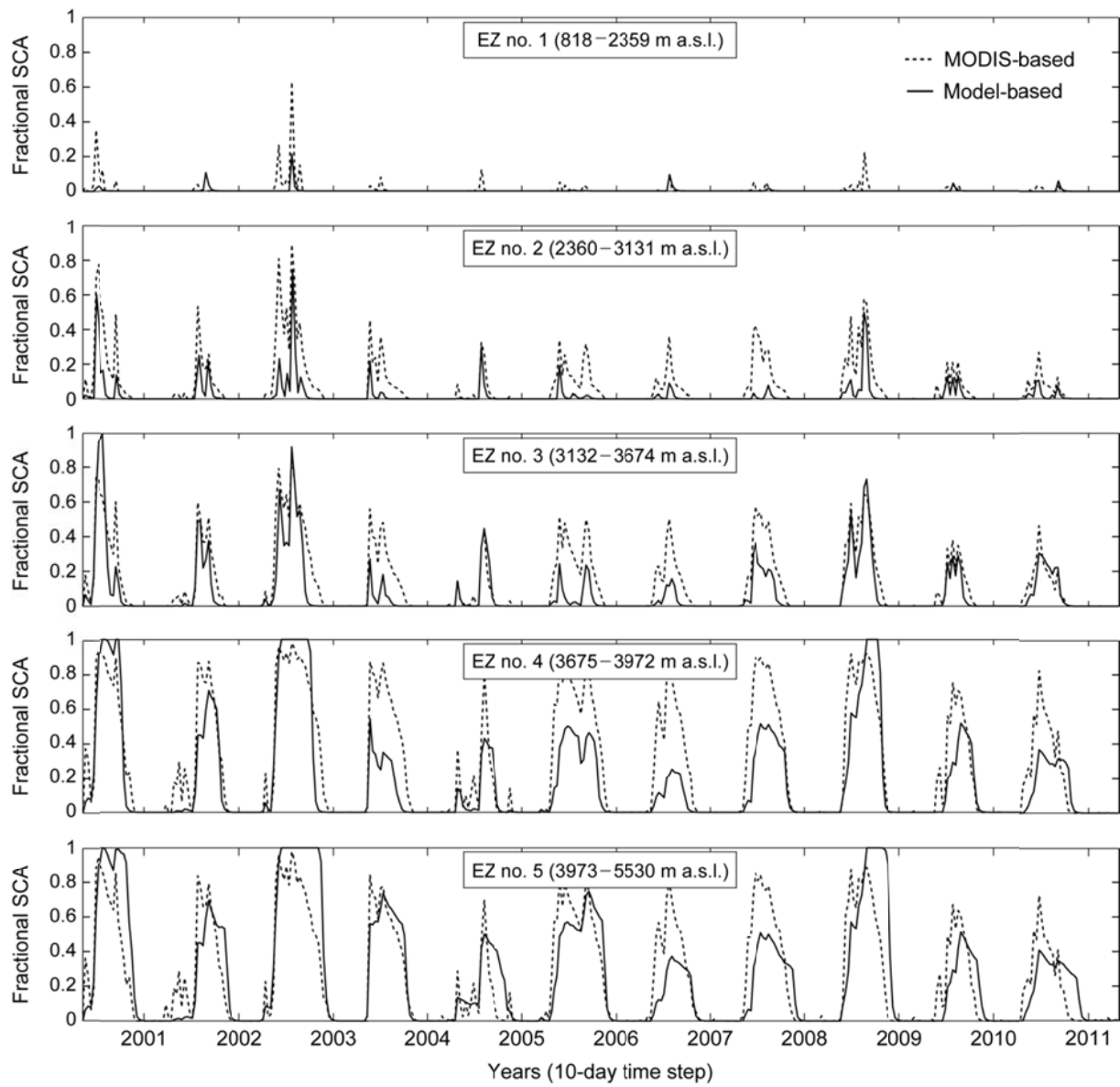
1482 **Figure 6** Comparison of simulated (i.e. Model C, accounting for sublimation) and observed (i.e. MODIS-based)
1483 fractional snow-covered areas (validation period). The graduations on the x -axis indicate the 1st of January of
1484 each year.
1485



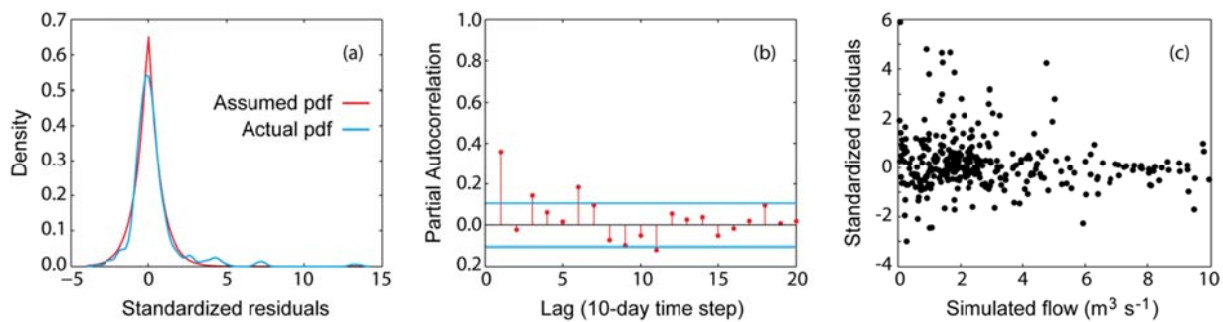
1486

1487

1488



1490 **Figure 7** Formal checks of the statistical assumptions used to describe model residuals. Application to Model C
1491 (simulated for the validation period with the inferred maximum likelihood parameter set): (a) assumed and actual
1492 pdf; (b) partial autocorrelation; and (c) heteroscedasticity of standardized residuals.
1493

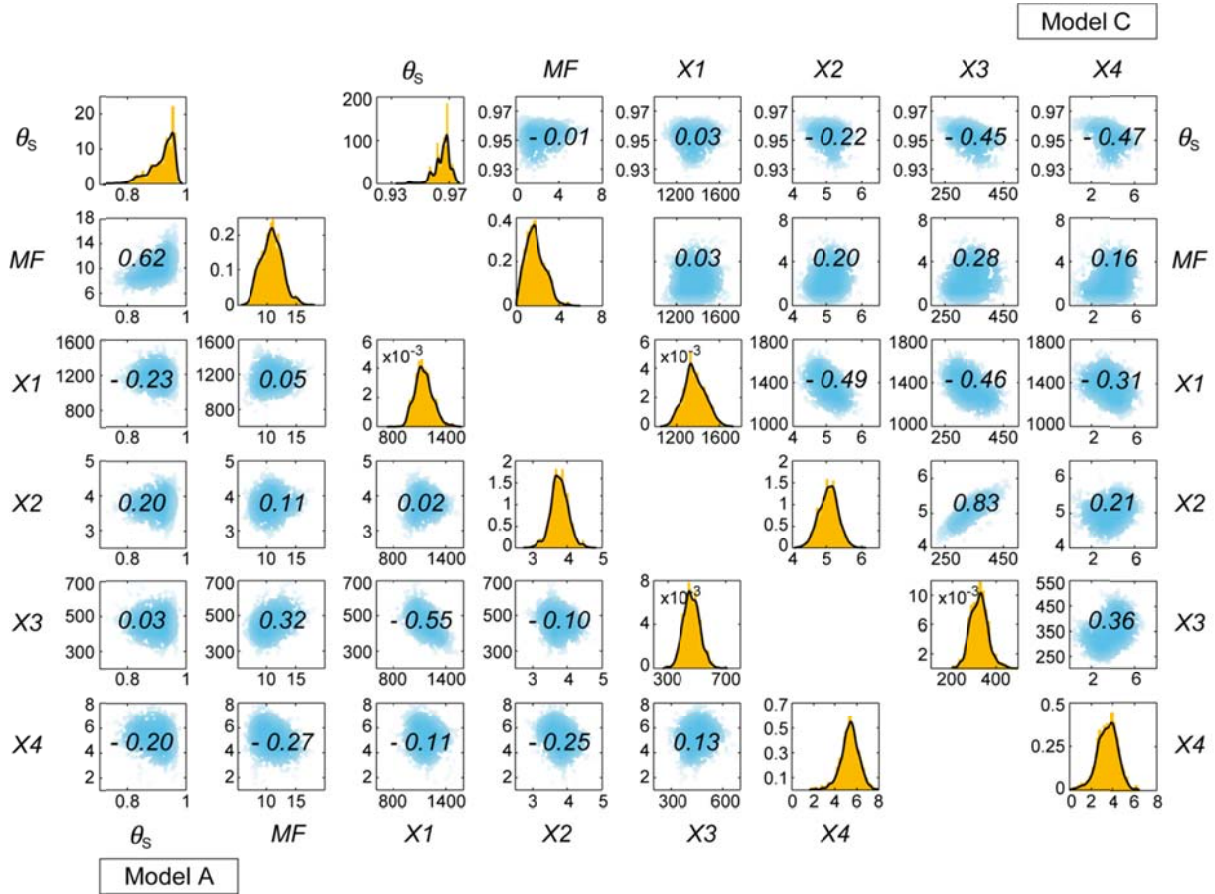


1494

1495

1496 **Figure 8** Two-dimensional scatter plots of the posterior parameter samples obtained with Models A and C. The
 1497 numbers in italic at the center of each cell indicate correlation coefficients. The histograms in orange represent
 1498 the marginal posterior distributions of parameters with superimposed kernel density estimates. The scatter plots
 1499 and histograms of Model B were not included here for brevity's sake, as they were very close to those of Model
 1500 C.

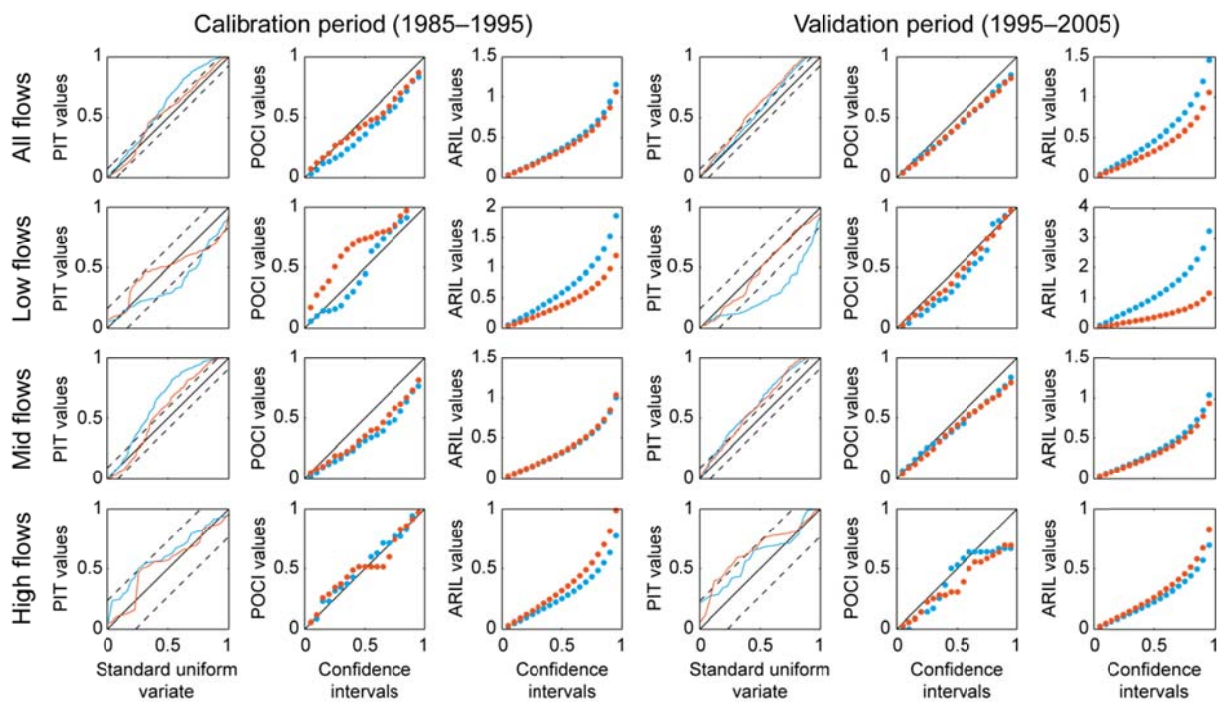
1501



1502

1503

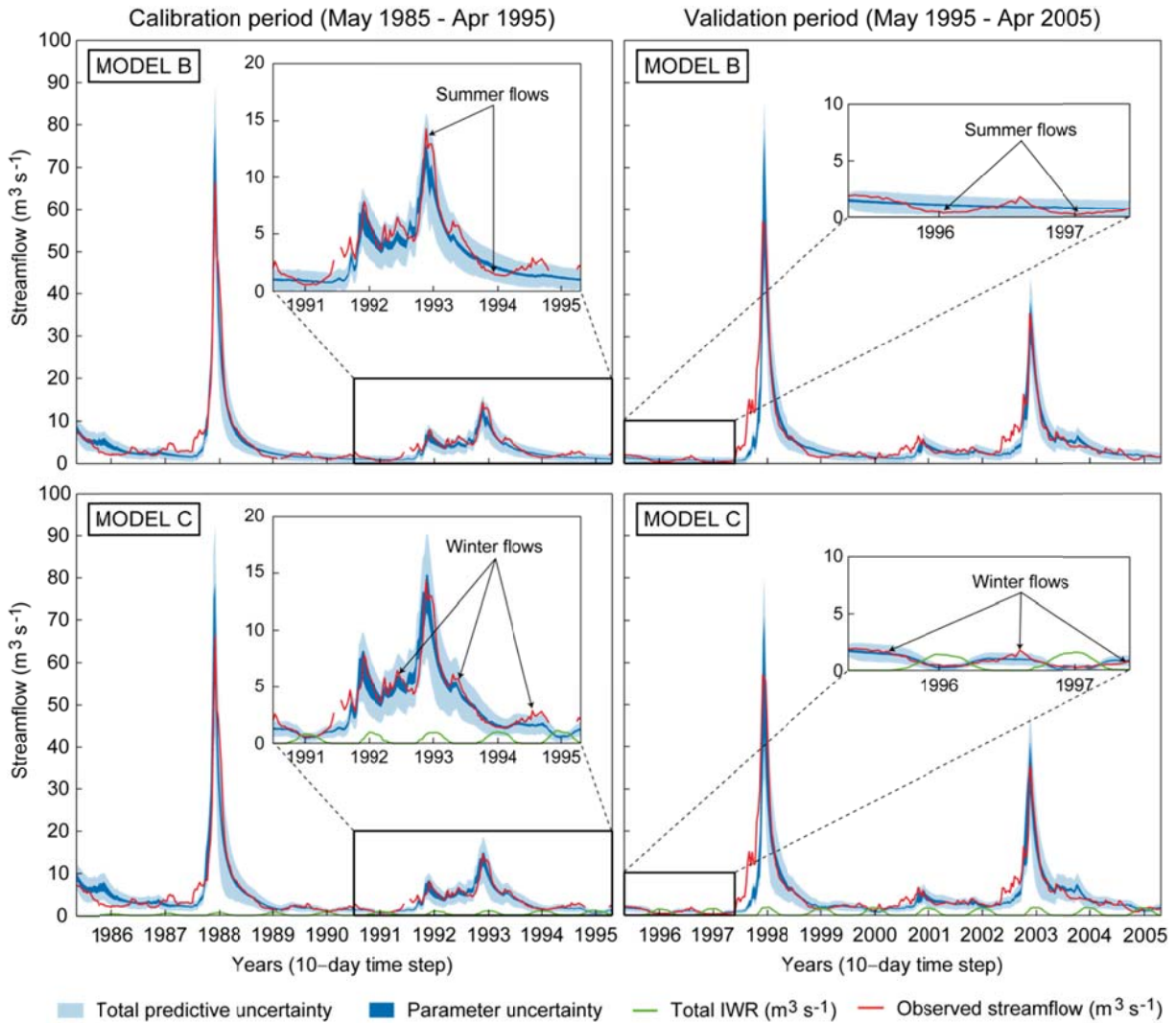
1504 **Figure 9** Posterior diagnostics used to evaluate the reliability (PIT, POCI) and resolution (ARIL) of the forecast
1505 distributions obtained with Model B (in blue) and Model C (in red).
1506



1507

1508

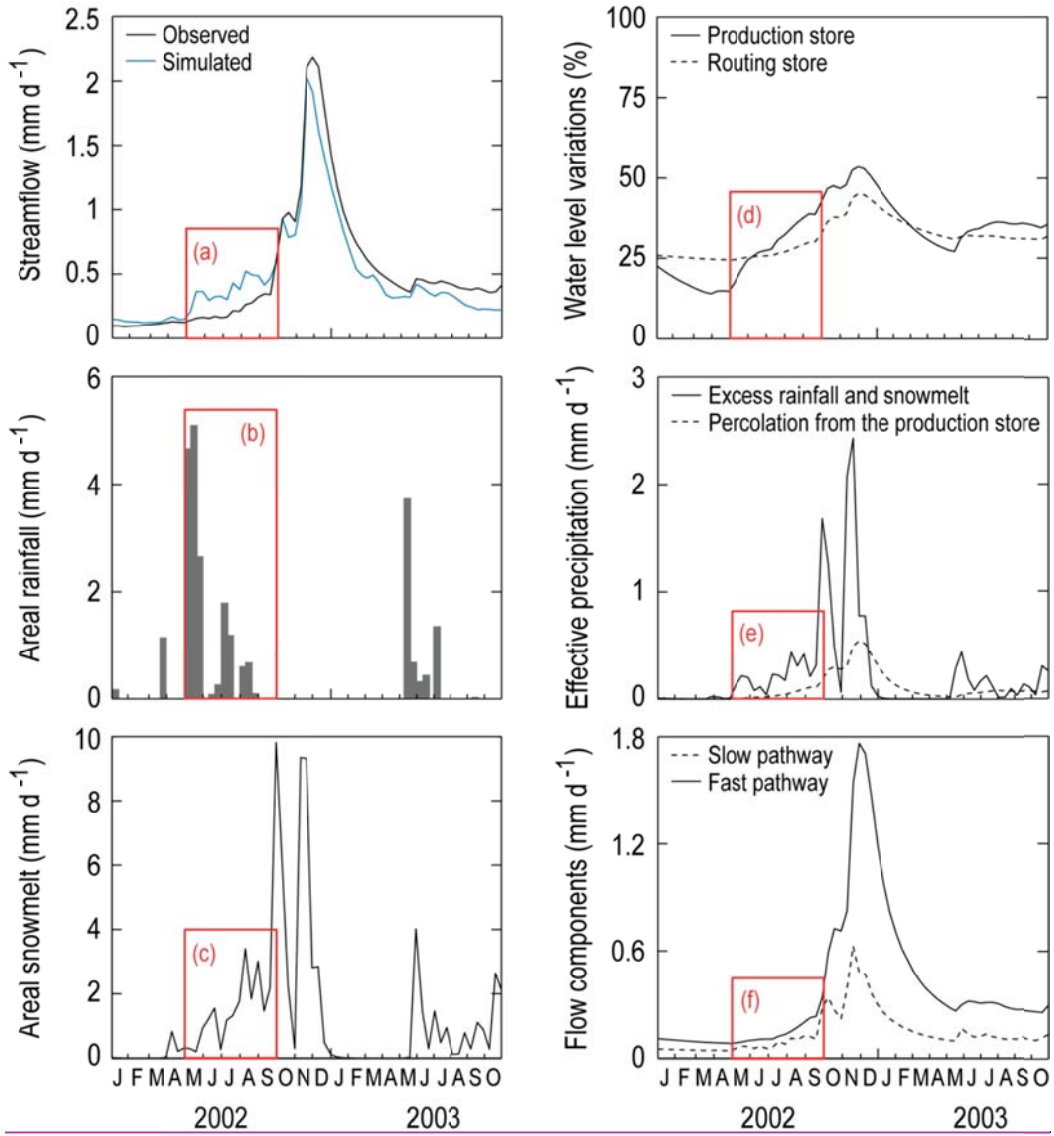
1509 **Figure 10** Predictive uncertainty bands obtained for both models with the DREAM algorithm and GL function.
 1510 The *dark blue* region represents the 95% confidence intervals associated with parameter uncertainty, whereas the
 1511 *light blue* region represents the 95% confidence intervals associated with parameter, model structure and input
 1512 errors. The graduations on the *x-axis* indicate the 1st of January of each year.
 1513



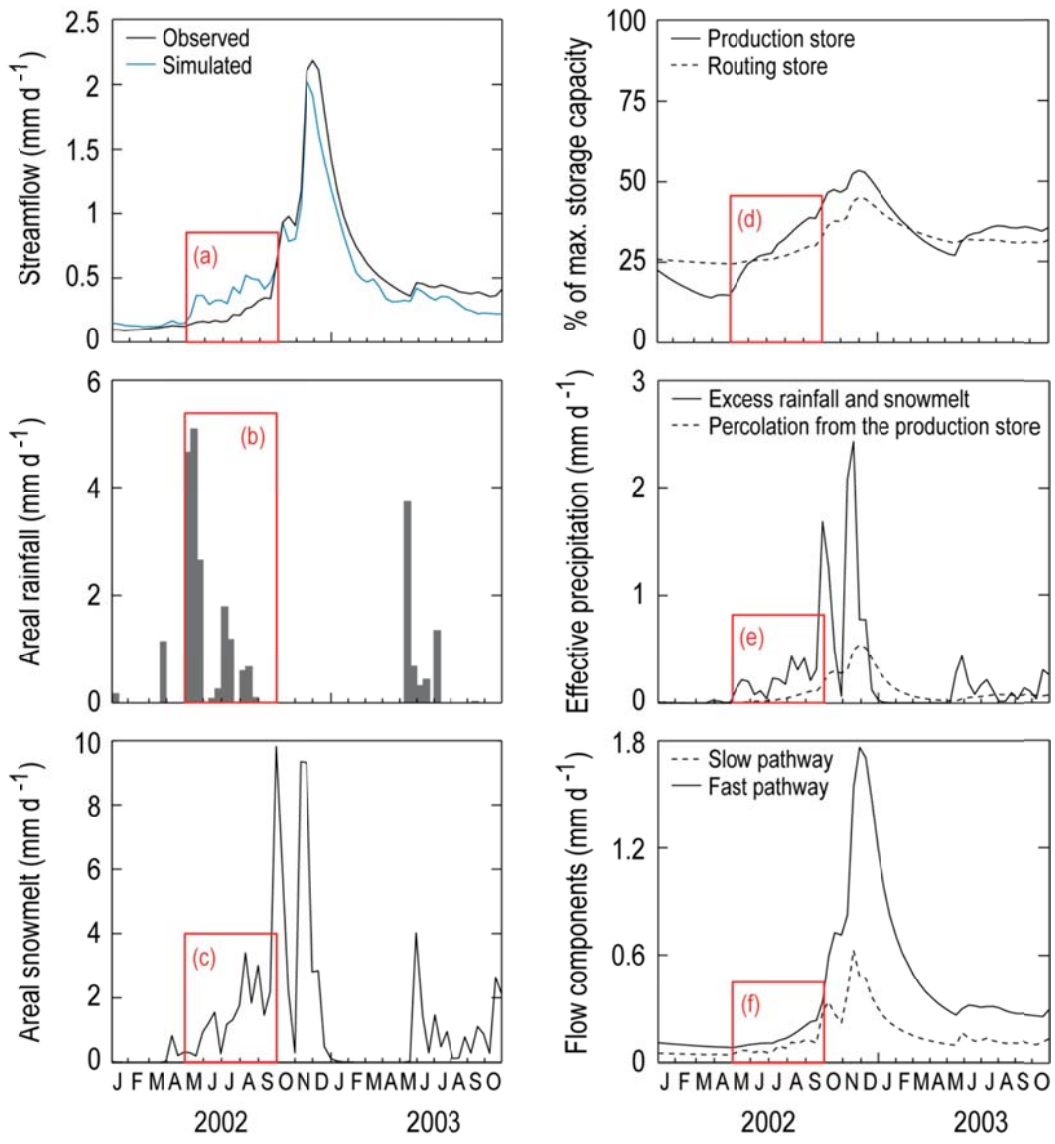
1514

1515

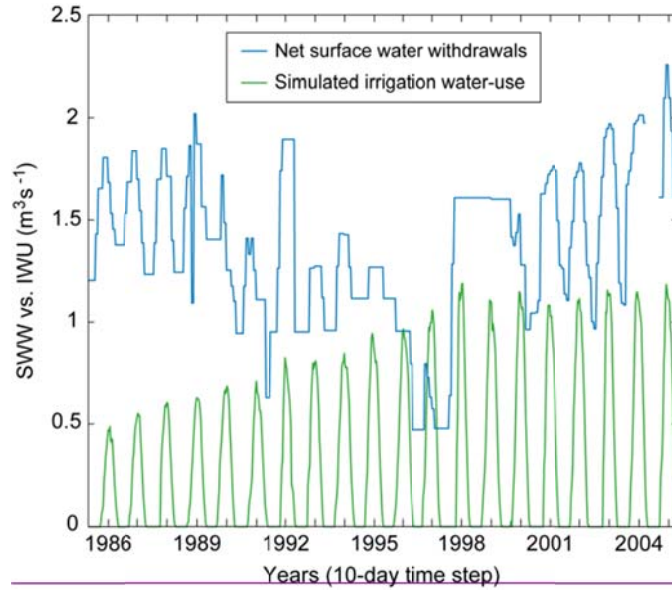
1516 **Figure 11** Internal state variables and fluxes obtained with Model C during the 2002–03 El Niño event (using
 1517 the best-performing parameter set obtained by calibration against the F_{obj} function).
 1518



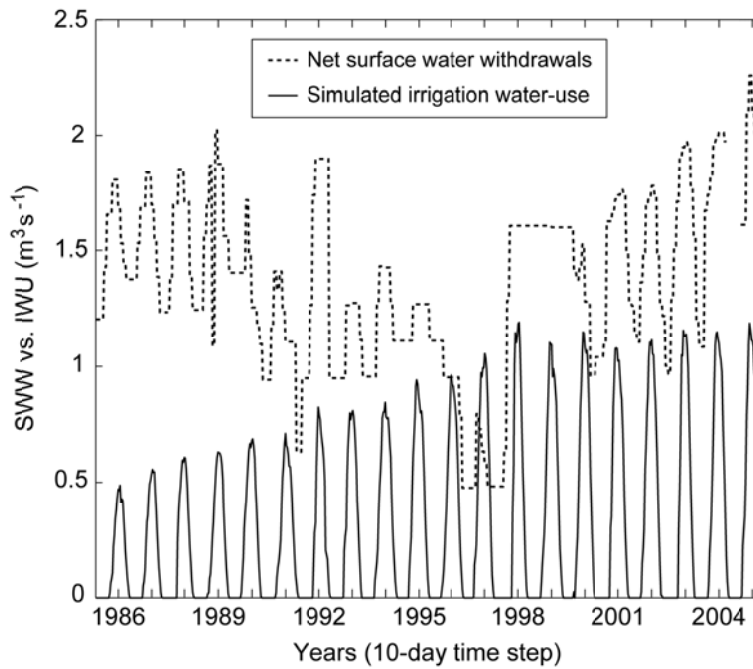
1519
 1520
 1521



1523 **Figure 12** Comparison of net surface-water withdrawals (SWW) and irrigation water-use (IWU) at the
1524 catchment scale: SWW were obtained by considering monthly restrictions to water access entitlements provided
1525 by the Chilean authorities, a conveyance efficiency of 0.6 and a field application efficiency of 0.6 for pisco
1526 varieties and 0.9 for table varieties; IWU was obtained from model simulations.
1527



1528
1529
1530



1531